Palaeontologia Electronica
palaeo-electronica.org

A new small-bodied longipterygid (Aves: Enantiornithes) from the Aptian Jiufotang Formation preserving unusual gastroliths

Jingmai O'Connor, Xiaoli Wang, Alexander Clark, Pei-Chen Kuo, Ryan Davila, Yan Wang, Xiaoting Zheng, and Zhonghe Zhou

ABSTRACT

The Longipterygidae are a diverse group of small to medium sized enantiornithine birds with elongate rostra and distally restricted dentition known from the Early Cretaceous Jehol Lagerstätten. The largest taxon, *Longipteryx,* is known from dozens of specimens but comparatively little is known about small-bodied taxa, sometimes resolved in a subclade, the Longirostravinae. Here we describe a small longipterygid representing a new taxon, *Chromeornis funkyi* gen. et sp. nov., with a combination of features present in longirostravines and *Longipteryx*. Cladistic analysis indicates the new species is a member of the Longipteryginae, more closely related to *Longipteryx* than other longipterygids. The specimen preserves extensive soft tissue including traces of the eyes, skin, and feathers, as well as an unusual mass of gastroliths preserved appressed against the left lateral margin of the cervical vertebrae. Computed-tomography based comparison with the in situ gastric mill preserved in the sympatric ornithuromorphs *Archaeorhynchus* and *Iteravis* strongly suggests these gastroliths are not gizzard stones. The absence of a gastric mill in enantiornithines is consistent with pectoral girdle morphology that indicates limited flight capabilities in Early Cretaceous species suggesting ground take off, a necessity of collecting stones, was energetically costly compared to ornithuromorphs. Increases in body mass due to a large gastric mill may have further impeded volant locomotion resulting in a low cost-benefit tradeoff such that this structure was unlikely to evolve during early enantiornithine evolution.

Jingmai O'Connor. Negaunee Integrative Research Center, Field Museum of Natural History, Chicago, IL, 60605 USA (corresponding author). jingmai@fieldmuseum.org
Xiaoli Wang. College of Life Sciences, Linyi University, Linyi 276005, China; and Shandong Tianyu Museum of Nature, Pingyi 273300, China; and College of Earth Science and Engineering, Shandong University of Science and Technology, Qingdao 266590, China (corresponding author). wangxiaoli@lyu.edu.cn
Alexander Clark. Negaunee Integrative Research Center, Field Museum of Natural History, Chicago, IL,

https://zoobank.org/A390561E-2FA0-4952-A900-6CB35AF909F0

Final citation: O'Connor, Jingmai, Wang, Xiaoli, Clark, Alexander, Kuo, Pei-Chen, Davila, Ryan, Wang, Yan, Zheng, Xiaoting, and Zhou, Zhonghe. 2025. A new small-bodied longipterygid (Aves: Enantiornithes) from the Aptian Jiufotang Formation preserving unusual gastroliths. Palaeontologia Electronica, 28(3):a56.
https://doi.org/10.26879/1589
palaeo-electronica.org/content/2025/5712-longipterygid-enantiornithine-chromeornis

60605 USA; and Committee on Evolutionary Biology, University of Chicago, Chicago, IL, 60637 USA. adclark@uchicago.edu
Pei-Chen Kuo. Negaunee Integrative Research Center, Field Museum of Natural History, Chicago, IL, 60605 USA. pkuo@fieldmuseum.org
Ryan Davila. Negaunee Integrative Research Center, Field Museum of Natural History, Chicago, IL, 60605 USA. rdavila@fieldmuseum.org
Yan Wang. College of Life Sciences, Linyi University, Linyi 276005, China; and Shandong Tianyu Museum of Nature, Pingyi 273300, China. wangyan6696@lyu.edu.cn
Xiaoting Zheng. Shandong Tianyu Museum of Nature, Pingyi 273300, China. ty4291666@163.com
Zhonghe Zhou. Key Laboratory of Vertebrate Evolution and Human Origins, Institute of Vertebrate Paleontology and Paleoanthropology, Chinese Academy of Sciences, Beijing, 100044, China. zhouzhonghe@ivpp.ac.cn

Keywords: Longipterygidae; new genus; new species; Jehol Biota; regurgitalite; gastrolith; Aves; Avialae.

Submission: 7 June 2025. Acceptance: 1 November 2025.

INTRODUCTION

The enantiornithines are a diverse group of terrestrial birds known from Cretaceous deposits around the world, with the notable exception of Antarctica and continental Africa (Chiappe and Walker, 2002; O'Connor, 2022). Fossils reveal that these birds were primarily arboreal and occupied a considerable size range, with body masses estimated between 5g and >1500 g (Clark et al., 2024; Xing et al., 2020). By the time they appear in the fossil record in the 131 Ma Huajiying Formation, enantiornithines were already a diverse and successful group (at least five taxa have been described) (Liu et al., 2019; Wang et al., 2017; Zhang and Zhou, 2000), persisting until 66 Ma when they go extinct alongside non-avian dinosaurs (Clark et al., 2024). The recent discovery of a possible ornithuromorph in Upper Jurassic deposits suggests the divergence between these two ornithothoracine clades occurred before 149 Ma (Chen et al., 2025). Enantiornithines appear to be the dominant group of terrestrial birds throughout the Cretaceous but the vast majority of information about this clade comes from the Lower Cretaceous Jehol Lagerstätten in northeastern China (Zhou and Wang, 2024). These Hauterivian to Aptian aged deposits have produced approximately half of the entire known Cretaceous aviary and estimated more than 90% the total volume of specimens (Zhou and Wang, 2024).

In the Jehol Biota, enantiornithines account for approximately half the known diversity and are the most abundant clade in terms of the number of recovered specimens (Zhou and Wang, 2024). One of the first enantiornithine clades recognized from these deposits was the Longipterygidae, easily identified by their elongate rostra (~60% of the total skull length) and distally restricted dentition (Zhang et al., 2000). Since the first taxon, *Longipteryx chaoyangensis*, was named in 2000, three additional longipterygids have been described: *Longirostravis hani* (Hou et al., 2004), *Rapaxavis pani* (Morschhauser et al., 2009), and *Shanweiniao cooperorum* (O'Connor et al., 2009). The fragmentary taxon, *Boluochia zhengi*, first named in 1995 (Zhou, 1995), was later reassigned to this clade (O'Connor et al., 2011a). It is considered by at least one researcher to be the senior synonym of *Longipteryx* (Yun, 2019). However, we consider these to be distinct taxa based on the differences noted by O'Connor et al. (O'Connor et al., 2011a) although comparison is severely limited by the incomplete and poor preservation of the holotype and only known specimen of *Boluochia*. The Longipterygidae is generally considered to consist of two clades, the Longipteryginae *(Longipteryx* and *Boluochia),* which are proportionately larger with robust, recurved teeth, and the Longirostravinae *(Longirostravis, Rapaxavis,* and *Shanweiniao),* which are small-bodied birds with proportionately smaller teeth and no manual ungual phalanges (Stidham and O'Connor, 2021).

In the past 15 years, several junior synonyms of *Longipteryx* have been described (e.g., "Shenjingornis", "Camptodontornis") and several referred specimens have been reported (Li et al., 2010; Li et al., 2012; Wang et al., 2015). This taxon has been the subject of significant research, revealing its unusual, crenulated dentition (Wang et al., 2015) with hypertrophied tooth enamel (Li et al., 2020), the morphology of its quadrate (Stidham and O'Connor, 2021), and its diet (Clark et al.,

2023; O'Connor et al., 2024). In contrast, all other longipterygids are known from single specimens and very little is known about their biology although attempts have been made to infer diet through quantitative analyses (Clark et al., 2023; Miller et al., 2022). Here we describe a new small-bodied longipterygid that superficially appears morphologically intermediate between previously known longipterygines and longirostravines. We describe this new specimen, explore its relationship relative to other longipterygids through cladistic analysis, and investigate the significance of preserved soft tissues and the aggregate of gastroliths [sensu Wings (2007)] adjacent to the neck.

Institutional Abbreviations

DNHM, Dalian Natural History Museum, Dalian, P.R. China; IVPP, Institute of Vertebrate Paleontology and Paleoanthropology, Beijing, P.R. China; STM, Shandong Tianyu Museum of Nature, Pingyi, P.R. China.

MATERIALS AND METHODS

The holotype specimen STM7-156 is reposited at the Shandong Tianyu Museum of Nature in Pingyi, Shandong Province, China. The specimen was studied using an Olympus microscope and photographed using a Canon EOS 5D. We conducted x-ray fluorescence (XRF) elemental analysis of the gastrolith mass using a handheld ThermoFisher Scientific Portable XRF Analyzer Niton XL3t 950 Instrument S/N 93368. Principle component analyses of the chemical data were conducted using "murrap.gcg" created by the University of Missouri's Archaeometry Laboratory (Glascock, 2021). The gastrolith mass was scanned using the IVPP computed tomography (CT) scanner with a voxel size of 35 microns. The data was processed using VG Studio Max. Figures were produced using Adobe Illustrator 2024. Terminology primarily follows Baumel & Witmer (Baumel and Witmer, 1993). Cladistic analysis was performed using TNT (Goloboff et al., 2008).

SYSTEMATIC PALAEONTOLOGY

Class AVES Linnaeus 1758
Clade ORNITHOTHORACES Chiappe 1995
Clade ENANTIORNITHES Walker 1981
Family LONGIPTERYGIDAE Zhang et al. 2000
Chromeornis funkyi gen. et sp. nov.
Figures 1-4

zoobank.org/A3A5E6C9-9352-4235-A90C-A30466F60F4D

Genus *Chromeornis*

zoobank.org/2741EE88-74BF-4FED-BCD1-81E45DE2C545

Holotype. STM7-156, a nearly complete and articulated mature individual preserved in a slab and counterslab missing most of the pelvis and left pedal digits, also preserving soft tissues of the body, feathers and a large mass of gastroliths just adjacent to the cervical vertebrae.

Locality and Horizon. Lamadong Town, Jianchang County, Liaoning Province, China. Aptian (120 Ma) Jiufotang Formation.

Etymology. Funky Chromeo bird, in honor of the Chromeo Funklordz P-Thugg and Dave 1, who like many birds, make beautiful music. Pronounced crow-me-OR-niss funk-ee.

Diagnosis. A small (estimated 33.5 g) longipterygid (rostrum ~60% of the skull or greater, distally restricted dentition, premaxillary corpus with elongate imperforate rostral end with parallel dorsal and ventral margins, robust pygostyle longer than tarsometatarsus, coracoid with straight lateral margin, humerus with narrow deltopectoral crest) enantiornithine (cranially forked pygostyle with ventrolateral processes, Y-shaped furcula with dorsally excavated rami, proximal humerus with small convex humeral head separated from the dorsal and ventral tubercles by concavities, minor metacarpal projecting farther distally than the major metacarpal, metatarsal IV reduced) distinguishable by the unique combination of the following characters: dentary straight; sternum with slightly splayed lateral trabeculae with asymmetrical fan-shaped distal expansions and short, straight intermediate trabeculae; hand shorter than humerus; alular digit short with small claw; second phalanx of major digit half the length of first phalanx; femur straight.

Differential diagnosis. STM7-156 can be distinguished from the previously described *Longipteryx* in having a straight ventral margin of the dentary; it differs from *Longirostravis* and *Rapaxavis* in having simple, unforked distal expansions of the lateral sternal trabeculae and straight intermediate trabeculae; it differs from *Longipteryx* and *Rapaxavis* in having projecting intermediate trabeculae; it differs from *Longipteryx* and *Shanweiniao* in having a proportionately shorter alular digit; it differs from *Rapaxavis* in having a claw on the alular digit; it differs from *Longirostravis, Rapaxavis,* and *Shanweiniao* in having a claw on the major digit (second manual phalanx sharply tapered in *Longirostravis* and *Rapaxavis* and more tapered in *Shanweiniao* than in STM7-156); it differs from all previous longipterygids in having an intermembral index

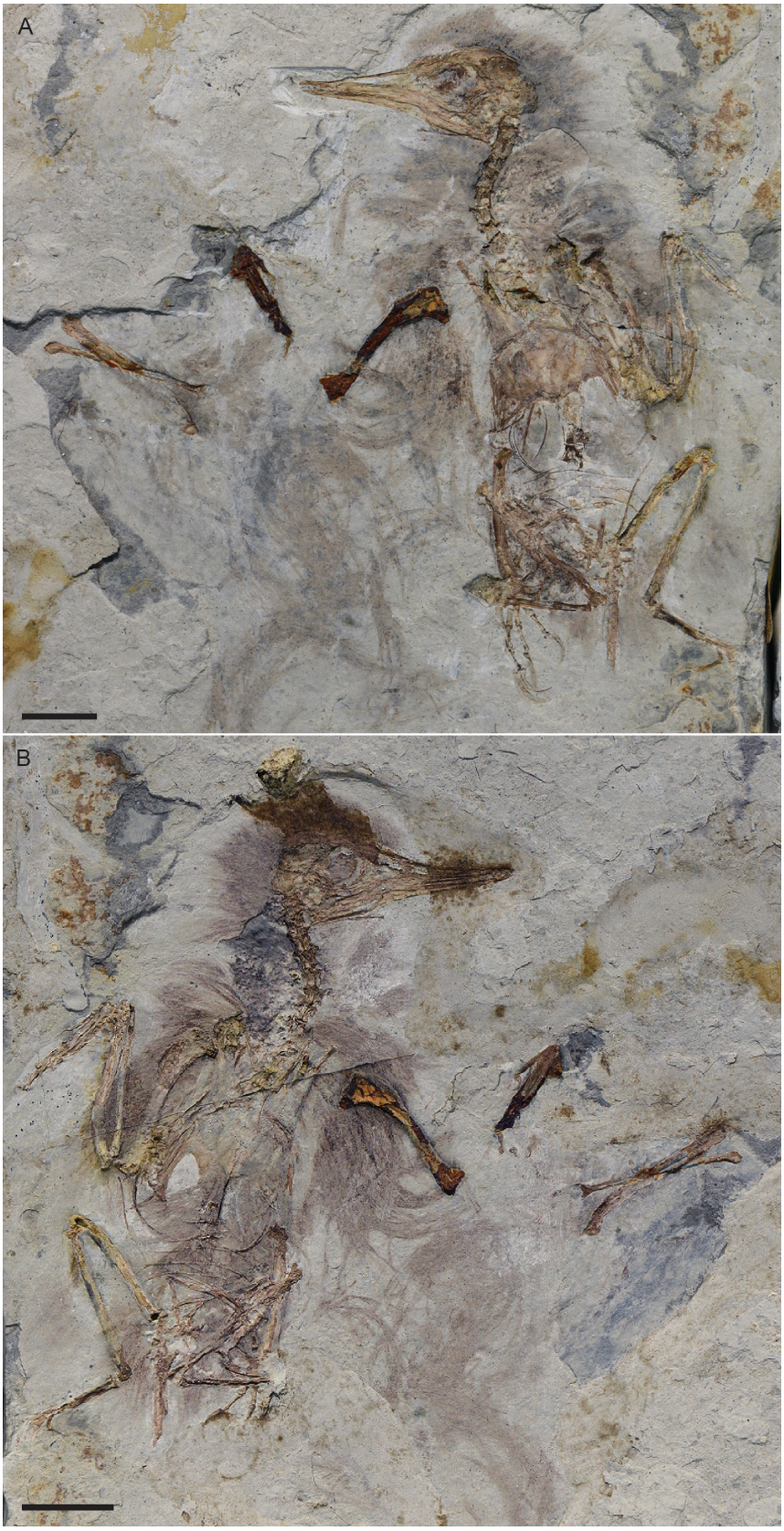

FIGURE 1. Photographs of the slab (A) and counter slab (B) of *Chromeornis funkyi* gen. et sp. nov. STM7-156. Scale bars equal one centimeter.

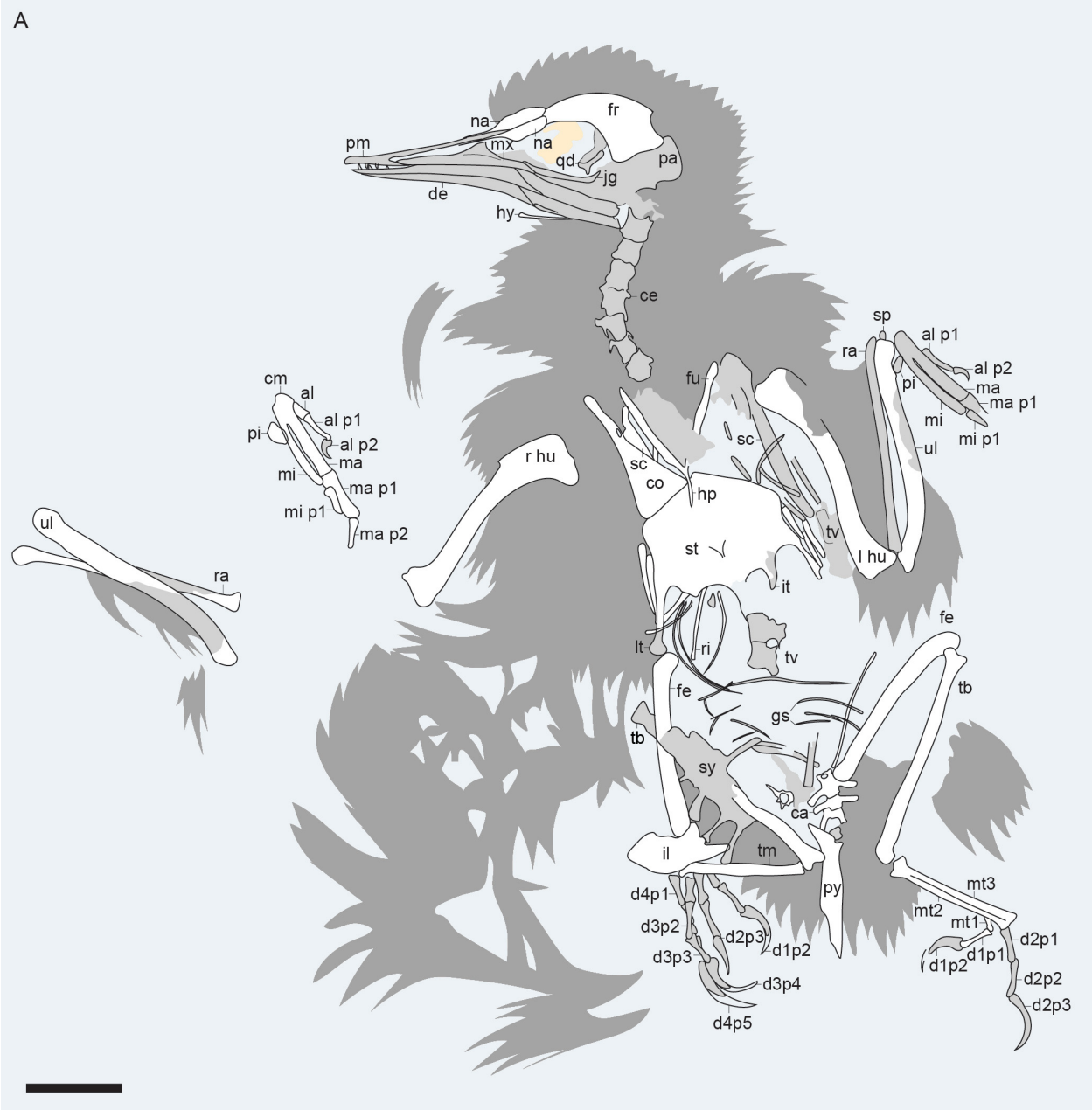

FIGURE 2. Line drawing of the slab (A) and counter slab (B) of *Chromeornis funkyi* gen. et sp. nov. STM7-156. Anatomical abbreviations: al, alular metacarpal; ca, caudal vertebrae; ce, cervical vertebrae; cm, carpometacarpus; co, coracoid; d1-4, pedal digits 1-4; de, dentary; fe, femur; fr, frontal; fu, furcula; gs, gastralia; gt, gastroliths; hp, hypocleidium; hu, humerus; hy, hyoid; il, ilium; it, intermediate trabecula; jg, jugal; kl, keel; lt, lateral trabecula; ma, major metacarpal; mi, minor metacarpal; mt1-4, metatarsals 1-4; mx, maxilla; na, nasal; p1-5, phalanges 1-5; pa, parietal; pi, pisiform; pm, premaxilla; pu, pubes; py, pygostyle; qd, quadrate; ra, radius; ri, ribs; sc, scapula; sp, scapholunare; st, sternum; sy, synsacrum; tb, tibiotarsus; tm, tarsometatarsus; tv, thoracic vertebrae; ul, ulna; xp, xiphoid process. White indicates well-preserved or moderately well-preserved bone; medium grey represents feathers; dark grey indicates the mass of gastroliths; peach indicates other soft tissues (melanin in the eye and skin). Scale bars equal one centimeter. (Continued on next page.)

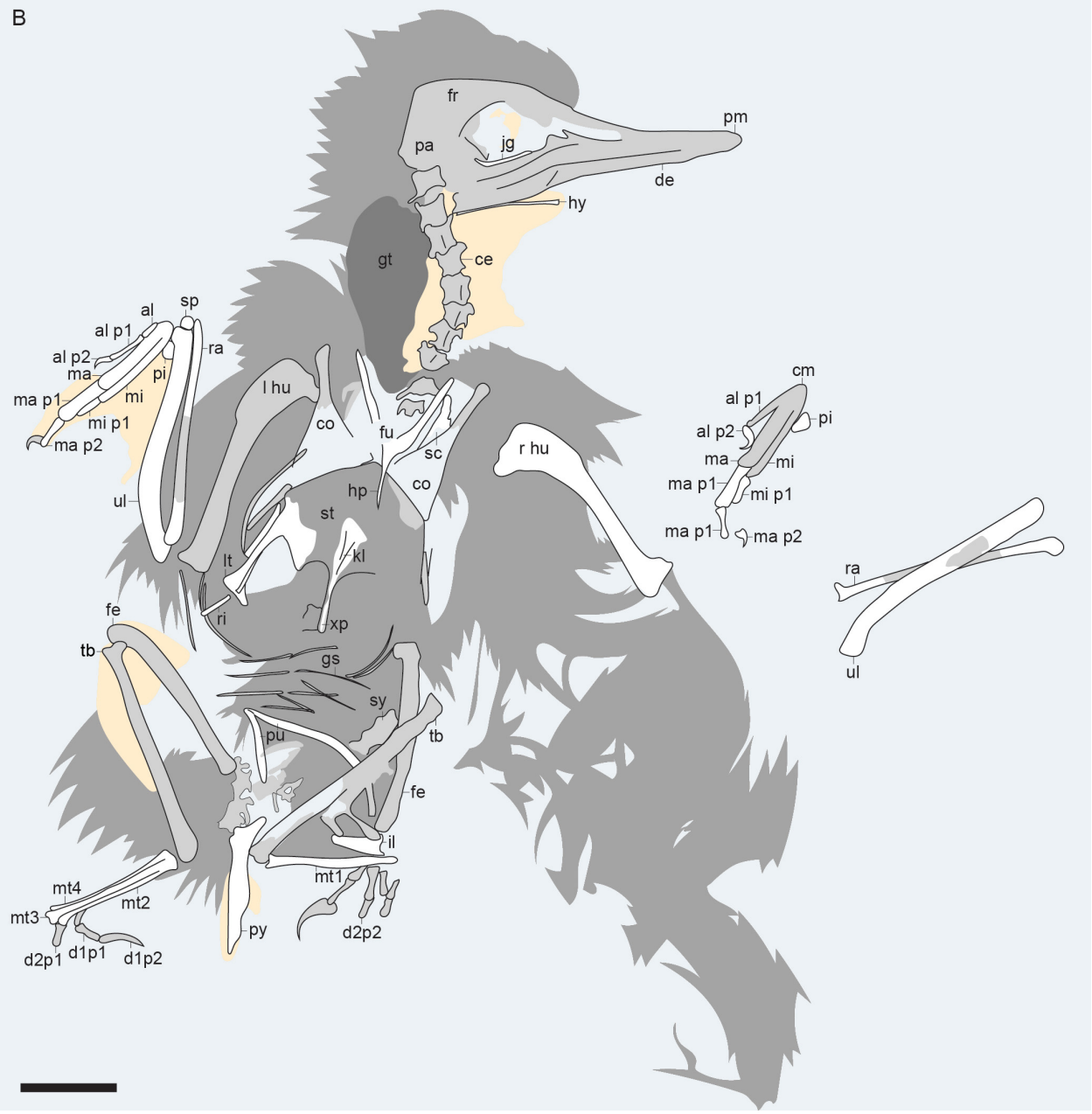

FIGURE 2 (continued from previous page).

(humerus + ulna/femur + tibiotarsus) of 1.14, intermediate between *Rapaxavis* (1.09) and *Longirostravis* (1.07) and *Shanweiniao* (1.23), but within the range of longirostravines and with much shorter forelimbs than observed in *Longipteryx* (1.44-1.51) (Table 1). Additional comparison with *Shanweiniao* and *Longirostravis* is hindered by poor preservation of the only known specimens of these taxa.

DESCRIPTION

The skeleton, though nearly complete, is poorly preserved, with all the bones split between the slab and counterslab. The bones are mostly in articulation except for the right forelimb and the pelvis, which is disarticulated although the hindlimbs remain in situ. By humeral length, STM7-156 is the smallest known longipterygid but it is close in size to *Shanweiniao, Rapaxavis,* and *Longirostravis* (Tables 1, 2).

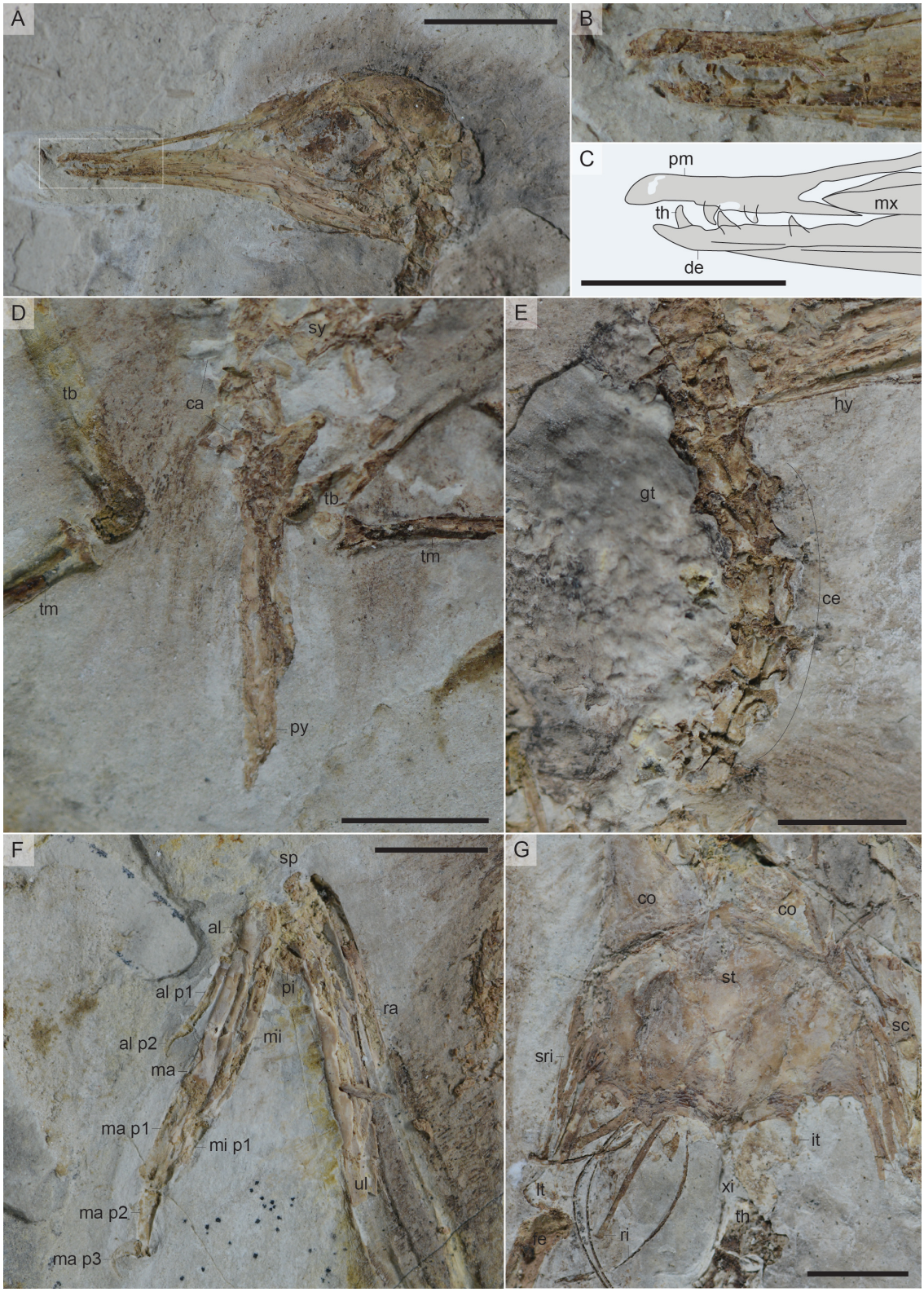

FIGURE 3. Close up photographs of key morphologies preserved in STM7-156. A, skull (main slab); B-C, close-up of the tip of the rostrum (main slab) and interpretative drawing showing the proportionately large teeth; D, impression of the neck (counterslab); E, pygostyle (counterslab); F, left forelimb (counterslab); G, sternum (main slab). Scale bar is one centimeter in A; scale bar is five millimeters in B-G. Anatomical abbreviation not listed in Figure 2 caption: sri, sternal ribs.

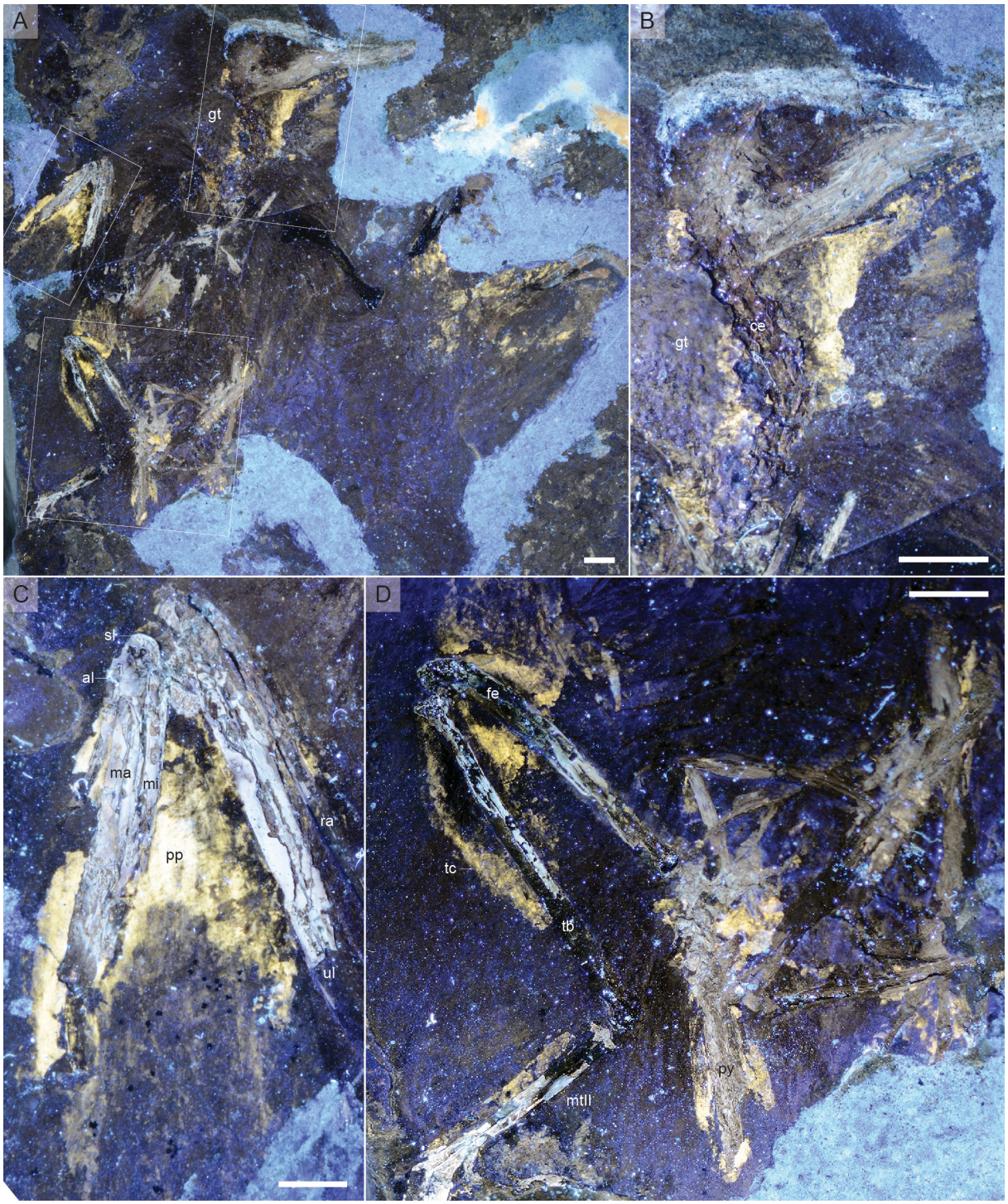

FIGURE 4. Soft tissues in the main slab of STM7-156 photographed under UV light. A, full slab, rectangular boxes indicate regions magnified in B-D; B, close up of the neck region, showing the gastrolith mass overlying the dorsal trace and the ventral traces forming a small gular expansion; C, close up of the left wing showing the postpatagium and a narrow margin of soft tissue along the cranial margin of the hand; D, close up of the caudal half of the skeleton showing the soft tissue outline preserved on the right hindlimb, which suggests the mm. *iliotibialis lateralis* and *iliofibularis* were smaller than in neornithines, and the characteristic 'drumstick' shape of the mm. *tibialis cranialis* (cranial surface) and *gastrocnemius* (caudal surface) – soft tissue is also visible preserved surrounding the pygostyle and along the dorsal margin of the tarsometatarsus. All scale bars equal five millimeters. Anatomical abbreviation not listed in Figure 2 caption: pp, postpatagium; sl, semilunate carpal; tc, *tibialis cranialis* muscle.

TABLE 1. Select measurements from STM7-156. Measurements in millimeters. Asterix indicates estimates.

Skull length	30.7
Rostral length	18.2
Synsacrum	15.5
Pygostyle	13.1
Coracoid length	12.3
Coracoid, sternal width	5.6
Furcula, ramus length	8.8
Furcula, hypocleideum length	5.8
Interclavicular angle	55.5˚
Sternum, length	16.2
Sternum, width (distal expansions, lateral trabeculae)	20
Humerus, length	20.9
Humerus, deltopectoral crest	6.3
Ulna	23.7
Radius	22.1
Carpometacarpus	9.9
Alular metacarpal	1.8
Alular metacarpal, phalanx 1	3.2
Alular metacarpal, phalanx 2	1.7
Major metacarpal	8.3
Major metacarpal, phalanx 1	4.3
Major metacarpal, phalanx 2	2.8
Major metacarpal, phalanx 3	1.8
Minor metacarpal	9.3
Minor metacarpal, phalanx 1	2.7
Ilium	10.5*
Pubis	15.3
Femur	17.7
Tibiotarsus	21.3
Tarsometatarsus	13.1

Skull

As in other longipterygids, the rostrum is elongated. Previously, longipterygids were diagnosed as having a rostrum that forms approximately 60% or more of the skull (O'Connor et al., 2009). In STM7-156 the rostrum measures 59% in the main slab and 60% in the counterslab, similar to the proportions observed in *Rapaxavis* (Table 2). The imperforate region of the premaxilla distal to the external nares (premaxillary corpus) is long and narrow with parallel dorsal and ventral margins, a longipterygid synapomorphy (O'Connor et al., 2011a) (Figures 1-3). The slight concavity on the dorsal margin reportedly present in other longipterygids is very weakly developed (O'Connor et al., 2011a). The nasal (frontal) processes are elongate, reaching the rostral margin of the antorbital fenestra and forming a wedge-like articulation between the elongate nasals. The left and right premaxillae each preserve a single tooth but in a different position indicating at least two teeth were present (Figure 3B, C); their spacing suggests the premaxillae would each bear four teeth as in *Longipteryx* and most toothed birds (O'Connor and Chiappe, 2011). The teeth are mesiodistally elongate at the base, apically tapered, and recurved, resembling the condition in *Longipteryx* (Zhang et al., 2001).

The nasals articulate with the nasal (frontal) processes of the premaxilla for half their length. The premaxillary process is long, thin, and sharply tapered. Slightly rostral to the caudal margin of the nasal processes of the premaxilla, the body of the nasals expands laterally, presumably to contact the ascending (nasal) process of the maxilla and form the caudal margin of the external nares, as in *Longipteryx* (O'Connor and Chiappe, 2011). The nasal is widest level with the caudal margin of the premaxilla, tapering gently caudally towards the articulation with the frontals. It appears that caudal to the articulation with the premaxilla, the nasals contacted medially and formed a wedge-like articulation between or overlapping the frontals.

Like other longipterygids, the maxilla has an elongate premaxillary process that is approximately twice the length of the jugal process (Figures 1-3). Only the ventral portion of the ascending process is preserved as a triangular sheet of bone that may be perforated rostrally by a maxillary (or promaxillary) foramen. The dorsal contact with the nasal is not preserved. The jugal ramus forms a caudoventrally sloping articulation with the jugal. As in other longipterygids, maxillary teeth are absent. The lacrimal is not preserved. The jugal is slightly bowed so that the dorsal margin is gently concave. Caudally it appears unforked with only a caudodorsally oriented ‘postorbital’ process. The external naris is demarcated by the premaxilla rostrally and dorsally, the maxilla ventrally, and the nasal dorsally and caudally. The rostral two thirds of the dorsal margin is formed by the nasal process of the premaxilla and the caudal third is formed by the nasals.

The exposed left frontal is long, rostrally narrow, and caudally expanded forming the ‘petal’ shape characteristic of other enantiornithines. It appears to have a blunt postorbital process developed at the caudolateral margin. The frontal is

TABLE 2. Comparative measurements of longipterygid taxa. Body mass was calculated from humeral length based on the formula presented by Liu et al.(Liu et al., 2012).

Taxon	Collection No.	Skull	Rostrum	Rostrum: Skull	Humerus	Skull: Humerus	Femur	Tibiotarsus	Inter-membral index	Body mass
Chromeornis	STM7-156	30.7	18.2	0.59	20.9	1.47	17.7	21.3	1.14	33.5
Longipteryx	IVPP V12325	55	~35.5	0.61	42	1.31	28.3	30	1.51	119.3
Longipteryx	IVPP V12552	48.6	29.7	0.61	39.4	1.23	27	28.3	1.44	100.6
Longipteryx	DNHM D2889	67.7	48.5	0.72	50.6	1.34	30	39.6	1.47	155.5
Longirostravis	IVPP V13309	32.9	24.6	0.75	23.5	1.40	20	25	1.07	42.6
Shanweiniao	DNHM D1878	32.4	19.6	0.60	22.4	1.45	17.6	22.5	1.23	37.9
Rapaxavis	DMNH D2522	30.4	17.8	0.59	23.6	1.29	19.1	24	1.09	44.1

unfused to the rectangular (mediolaterally wider than dorsoventrally tall) parietal. The left quadrate is poorly preserved, but it is angled so that the mandibular condyles are rostral to the otic process.

The dentaries are straight and elongate. They become dorsoventrally narrower at their tips similar to *Longirostravis* and *Rapaxavis*, whereas they are bowed ventrally in *Longipteryx* (Clark et al., 2023). The rostrodorsal margin is sharply tapered as in *Longipteryx, Rapaxavis,* and possibly also *Longirostravis* (O'Connor et al., 2024). The dentaries are dorsoventrally thickest at the point of rostral contact with the surangular, after which the dentary forms an unforked caudoventrally sloping articulation with the postdentary bones. Three teeth can be clearly identified in the right dentary. As in longipterygids, these are apically tapered, recurved, and basally expanded. The teeth are proportionately larger than *Longirostravis* and *Rapaxavis*; the rostral-most dentary tooth appears to have a crown height nearly equal to the depth of the dentary, as in *Longipteryx* (less than dentary depth in *Rapaxavis* and *Longirostravis*) (Hou et al., 2004; O'Connor and Chiappe, 2011).

Only the angular and surangular can be clearly identified. The surangular is approximately 2.5x the dorsoventral thickness of the angular. The mandibular cotyle is deeply concave. A single hyoid bone is preserved. It is rostrally expanded, as in *Longipteryx* (O'Connor et al., 2025b), suggesting the presence of an ossified but unpreserved basihyal.

Axial skeleton

Eight cervical vertebrae are preserved not including the atlas indicating there were at least nine cervicals, as in *Rapaxavis* and *Longipteryx* (O'Connor et al., 2011c; Zhang et al., 2001). The fourth-sixth preserved vertebrae are the longest (Figures 1-3). The seventh and eighth are approximately equal in length and width. Voids visible in the counterslab indicate the ventral surfaces of the vertebrae were sharply keeled with a midline ridge extending the entire length of the centra, also observed in *Rapaxavis* and *Longipteryx* (Figure 3E). The postzygapophyses are longer than the prezygapophyses, as in *Rapaxavis* and *Longipteryx*. The cranial end of each cervical vertebra is wider than the caudal end such that the prezygapophyses are located more laterally than the postzygapophyses.

Three poorly preserved thoracic vertebrae are preserved distal to the left scapula and two more articulated vertebrae are preserved near the sternal xiphoid process. They have spool-shaped, laterally excavated centra with flat articular surfaces, typical of enantiornithines (Chiappe and Walker, 2002). The vertebrae have tall neural spines and postzygapophyses that extend beyond the caudal articular surface.

The synsacrum is poorly preserved but seven vertebrae can be discerned, as in other longipterygids. It gently increases in mediolateral width, being widest at the fourth and fifth vertebrae after which it narrows distally. The fifth vertebra bears robust processes that would have braced the ilia. The transverse processes on the last two sacrals are elongate and expanded at their distal ends, as in *Rapaxavis* and *Longipteryx*. In the penultimate sacral this process is laterally oriented, whereas it is weakly caudolaterally oriented in the last sacral, as in *Rapaxavis* (O'Connor et al., 2011c).

Four free caudal vertebrae are clearly preserved. Another two poorly preserved caudals are

tentatively identified. Of the clearly preserved vertebrae, one is disarticulated and exposed in cranial or caudal view; the other three are ventrally exposed in the main slab nearly in articulation with each other and the pygostyle. The vertebral canal is large and round, approximately 3.5x the size of the articular surface. A small neural spine is present. The transverse processes are 1.5x the width of the centrum and very slightly caudally oriented, as in *Longipteryx* and *Rapaxavis*, and typical of enantiornithines in general. Prezygapophyses are approximately 2/3 the length of the centrum in the first articulated caudal. The ventral surface appears to have been grooved. The caudal articular surface in the second articulated vertebra appears flat.

The pygostyle is typical of enantiornithines in morphology and longiptergyids in proportions, being robust and equal to the length of the tarsometatarsus (Figure 4D) (O'Connor et al., 2011a; O'Connor, 2022). It has well developed ventrolateral processes that extend proximally well beyond the articular surface with the last free caudal. The ventrolateral processes end abruptly so that the distal third of the pygostyle appears constricted, as in all longipterygids (O'Connor et al., 2011a). The cranial processes appear very small.

Ribs and gastralia

Three sternal ribs are preserved in articulation with the right costal margin on the sternum (Figure 4G). Four articulated sets of gastralia are visible caudal to the sternum and cranial to the pelvis. Each set consists of four elements. The first set appears to articulate with the distal end of the xiphoid process as observed in some enantiornithines (O'Connor et al., 2015).

Pectoral girdle and limb

The furcula is Y shaped as in other enantiornithines (O'Connor, 2022) and very similar to the condition in *Rapaxavis* with straight furcular rami demarcating an angle of 55˚ (51˚ in *Rapaxavis*) that are unexpanded omally. Although poorly preserved, it is clear that the dorsal surface of the furcular rami is deeply excavated, typical of enantiornithines, and it appears the rami would have had a V-shaped cross-section near their midpoints (Chiappe and Walker, 2002). The mediolaterally compressed hypocleidium is preserved articulating with the sternum, measuring two-thirds the length of the furcular rami (Figures 1, 2).

The coracoid is fan-shaped; the omal half is straight and narrow and the sternal half expands into a broad triangular pterygoma with straight medial, lateral and sternal margins. The acrocoracoid, scapular cotyle, and glenoid are roughly aligned proximodistally, as in other enantiornithines (Chiappe and Walker, 2002). Visible on the right, the supracoracoidal nerve foramen is separated from the medial margin by a bony bar. A procoracoid process is absent as in all enantiornithines with the possible exception of *Protopteryx* (Zhang and Zhou, 2000). The scapulae are mostly covered by the coracoids and sternum, although an elongate acromion process is visible. The distal half of the left scapula is straight and bluntly tapered. These morphologies of the scapula and coracoid are consistent with other longipterygids.

The rostral margin of the sternum is defined by the two straight margins for articulation with the coracoids, demarcating an angle of 125˚, compared to 110˚ in *Rapaxavis* (O'Connor et al., 2011c). The coracoids are adjacent but slightly separated on the midline (Figure 4G). The lateral trabeculae are angled laterally so that the distal expansions are located lateral to the craniolateral margins of the sternum, as in *Longipteryx*. As in *Shanweiniao*, they do not quite extend to the level of the distal margin of the xiphoid process, the opposite condition preserved in *Longipteryx, Longirostravis,* and *Rapaxavis* in which the lateral processes are longer. The lateral trabeculae end in a small, fan-shaped expansion similar to the simple expansion present in *Longipteryx*, and contrasting with the complex, branching morphology in *Longirostravis* and *Rapaxavis*. The intermediate trabeculae are much shorter than the lateral trabeculae but well developed compared to *Longipteryx* and *Rapaxavis* in which they form only gentle swellings on the caudal sternal margin. They are only weakly curved medially compared to *Longirostravis* but this may be an artifact of incomplete preservation (Hou et al., 2004). The sternal body expands slightly just distal to the costal margin but a distinct lateral 'zyphoid' process is absent. The xiphoid process is straight and rod-like with a well-developed ventrally projecting keel that shallows as it extends onto the sternal body, forks, and disappears well below the sternal rostrum, morphologies typical of Early Cretaceous enantiornithines (O'Connor, 2022; Zheng et al., 2012).

As in other longipterygids, the humerus is gently sigmoidal due to a strongly developed ventral tubercle (O'Connor et al., 2024; O'Connor et al., 2009). The midline of the proximal margin bears a small convexity marking the humeral condyle, separated from the dorsal and ventral pro-

cesses by concavities, typical of enantiornithines (Chiappe and Walker, 2002). The ventral tubercle has a straight ventral margin and was separated from the humeral head by the capital incision in caudal view. The deltopectoral crest is narrow, less than the 1/3 the width of the humeral shaft at its midpoint, extending for less than 1/3 the length of the humerus, and ends abruptly distally, typical of longipterygids (O'Connor et al., 2024). The distal margin of the humerus is angled although a distally projecting flexor process is not observed.

Although crushed, the ulna appears twice as robust as the radius and strongly bowed proximally, typical of Mesozoic birds (O'Connor et al., 2011b). The ulna has a weakly developed olecranon process; the distal end is not well preserved. The proximal end of the radius is expanded forming a well-defined humeral cotyla. The distal end is expanded and rounded in ventral profile but compressed in lateral aspect. A large carpal preserved between the hand and the ulna on the left side is identified as the pisiform (ulnare). Another smaller carpal is preserved distal to the ulna and is identified as the scapholunare (radiale). The pisiform also appears preserved together with the disarticulated right hand.

The hand is shorter than the humerus as in *Rapaxavis* but opposite *Longipteryx*. The semilunate carpal appears fused to the major and minor metacarpals. The minor metacarpal is longer than the major metacarpal, extending well beyond its distal margin, as in other enantiornithines (Chiappe and Walker, 2002; O'Connor, 2022; O'Connor et al., 2011b). The alular metacarpal is small and unfused, measuring 0.22 the length of the major metacarpal, typical of enantiornithines, and half its craniocaudal thickness. The minor metacarpal is half the thickness of the major metacarpal in dorsal view. The alular digit bears a small, recurved claw; the claw is proportionately larger in *Longipteryx* (Zhang et al., 2001) but entirely absent in *Rapaxavis* and *Longirostravis* (Hou et al., 2004; Morschhauser et al., 2009). The proximal base of a claw appears to be preserved in *Shanweiniao* (O'Connor et al., 2009). The alular digit is reduced, ending well before the distal margin of the major metacarpal. This is intermediate between the proportions in *Longipteryx*, in which the distal third of the alular ungual extends beyond the major metacarpal, and *Rapaxavis*, in which the single alular phalanx only reaches the midpoint of the major metacarpal. The first phalanx of the major digit is straight and as robust as the major metacarpal, but not distinctly expanded and dorsoventrally compressed as in ornithuromorphs (Zhou and Zhang, 2001). The second phalanx is 65% the length of the first, less robust, and tapers distally where it articulates with a small, recurved claw, approximately the same size as that of the alular digit. In *Longipteryx*, the only other longipterygid known to have a major digit ungual, the claw is larger than that of the alular digit and the non-ungual phalanges are proportionately longer (Wang et al., 2015; Zhang et al., 2001). A single phalanx is preserved on the minor digit. It is the smallest phalanx in the hand, slightly shorter than the penultimate phalanx of the major digit. It is wedge-shaped so that its distal margin is half the width of its proximal margin.

Pelvic girdle and limb

The pelvis is incomplete and disarticulated from the axial column (Figures 1, 2). A single ilium is preserved as a void. Based on its position relative to the pubes we tentatively identify this as the right ilium. Similar to other enantiornithines, the preacetabular wing is more than twice the dorsoventral height of the postacetabular wing and approximately twice as long. The rostral margin is angular, demarcated by a straight rostrodorsal margin and a straight rostroventral margin meeting to define a 67˚ angle. This margin is much more rounded in *Rapaxavis* but further comparison is hindered by poor preservation of the ilium in other longipterygids. The ventral margin cranial to the acetabulum is gently concave. The pubic pedicel extends slightly farther ventrally than the ischiadic pedicel, typical of Mesozoic birds. The postacetabular wing is slightly tapered caudally and has a blunt distal margin, as observed in other longipterygids.

Both pubes are preserved in articulation with each other but missing their proximal ends. It appears they would also be nearly in articulation with the ilium, although this is obscured by the split preservation between the two slabs. Distally the pubes form a short symphysis. A pubic boot, like that present in *Longipteryx* (Zhang et al., 2001), is not visible. The pubic shafts are laterally bowed. The ischia are not preserved or cannot be clearly identified.

As in *Longipteryx*, the femur is nearly straight in lateral view, whereas it is often bowed in other Cretaceous birds including *Rapaxavis*. The distal end is deflected caudally at the level of the condyles. The femur is 83% the length of the tibiotarsus, which is greater than observed in *Rapaxavis* and *Longirostravis* (80%) but much less than *Longipteryx* (94-95%) (Table 2). The tibiotarsus has a

flat proximal articular surface (angled in some taxa such as *Soroavisaurus*). The medial condyle of the tibiotarsus is nearly twice as wide as the lateral condyle and they taper towards each other, as in *Rapaxavis* (O'Connor et al., 2011c); the condyles appear to be subequal in *Longipteryx* (Wang et al., 2015) (Figure 3D). The left fibula is preserved articulating with the tibiotarsus. It is proximally nearly as dorsoventrally deep as the tibia but rapidly tapers distally, typical of non-pengornithid enantiornithines, and is most likely incomplete.

The distal tarsals appear fused to the metatarsals forming a tarsometatarsus (Figure 3D). In lateral view the proximal articular surface of the tarsometatarsus is concave and it appears the caudal margin was slightly elevated relative to the cranial margin. A hypotarsus is clearly absent, as in other enantiornithines (O'Connor, 2022). Metatarsal IV is very narrow and ends approximately level with metatarsal II as in *Longirostravis* and *Rapaxavis*, whereas metatarsal IV is longer than III in *Longipteryx* (O'Connor et al., 2011a). The dorsal surface of metatarsal III is convex along the proximal portion of the shaft that is well preserved. The metatarsal II trochlea is angled so that the lateral condyle is distal to the medial condyle and slightly expanded. The left metatarsal I is partially preserved in the counterslab suggesting the ramus bearing the trochlea for digit I was projected from the shaft.

The right pedal digits in the main slab are most complete but not clearly preserved. Only in digit II can the proportions be clearly discerned revealing the penultimate phalanx is longer than the proximal phalanx, as in most enantiornithines and consistent with their arboreal habits (Hopson, 2001; Morschhauser et al., 2009). All the digits have large claws also preserving their keratinous sheaths. The third pedal claw appears to be the largest, whereas digit II-IV unguals appear similarly sized in *Longipteryx* and *Shanweiniao*.

Ontogenetic assessment

STM7-156 is determined to be morphologically mature or nearly so based on the complete ossification of the sternum including the well-developed intermediate trabeculae and the fusion of the distal tarsals to the metatarsals (O'Connor et al., 2025a). Information from early immature enantiornithines suggests that novel morphologies of the lateral trabeculae ossify early, before the appearance of the intermediate trabeculae (Zheng et al., 2012). Less clear, it appears the semilunate carpal is fused to the major and minor metacarpals and the proximal tarsals are fused to the tibia although the alular metacarpal is unfused to the major metacarpal (Figure 4). These elements fuse in the final stage (stage 3) of ontogenetic maturation in enantiornithines indicating STM7-156 is stage 2b or 3, sensu Hu & O'Connor (Hu and O'Connor, 2017; O'Connor et al., 2025a).

Soft tissues

Dark traces in the orbit may represent remnants of the eye preserved within the bounds of the scleral ring, which is not preserved (Figures 1, 3A). Similar traces have been reported in other enantiornithines from the Jehol deposits (Tanaka et al., 2017). Traces of feathers are preserved along the dorsal margin of the skull, beginning caudal to the external nares (Figure 3A). These feathers continue along the dorsal margin of the neck and extend along both shoulders and along the dorsal margin of the left humerus and along the left side of the body (Figures 1, 2). Many disarticulated clumps of feathers are preserved below the right forelimb, which is also disarticulated. These are long and narrow resembling feathers preserved in *Cruralispennia* (Wang et al., 2017) and some early immature enantiornithines (O'Connor et al., 2020); this shape has been interpreted as indicative of immature feathers, the narrow morphology due to the preservation of a keratinous sheath present during feather growth (O'Connor et al., 2020). This may indicate STM7-156 was in molt at the time of death. No flight feathers appear to be preserved.

Under UVA light extensive soft tissues are visible preserved along the dorsal and ventral margin of the neck, the left hand, the right leg, and surrounding the pygostyle (Figure 4). These traces are considered to represent fossilized skin. This is based on the extent of the traces caudal to the ulna, which exceeds that of avian musculature but consistent with the shape of the postpatagium, a structure composed of skin and connective tissue (Figure 4C) (O'Connor, 2025). However, in regions like the hindlimb and tail in which the skin closely overlies muscles, the skin can be used to make inferences about the underlying musculature. The postpatagium has been previously documented in *Archaeopteryx* (Martin and Lim, 2005), *Eoconfuciusornis* (Zheng et al., 2017), and two other enantiornithines (Liu et al., 2019; Navalón et al., 2015). The skin outline along the dorsal and ventral margins of the femur suggests more limited musculature compared to extant birds, which may be due to the proportionately smaller pelvis in enantiornithines providing less muscular attachment space resulting

in smaller mm. *iliotibialis lateralis* and *iliofibularis* (Vanden Berge and Zweers, 1993) (Figure 4D). The soft tissue outline on the proximal tibiotarsus show the 'drumstick' avian morphology characteristic of the mm. *tibialis cranialis* (cranial) and *gastrocnemius* (caudal). This morphology is unsurprising, also observed in *Orienantius* (Liu et al., 2019), and was likely present even in the earliest theropods. The skin surrounding the pygostyle indicates the absence of rectricial bulbs, as observed in *Orienantius* (Liu et al., 2019), providing additional support for the absence (or reduction) of this structure in enantiornithines (Wang and O'Connor, 2017). Exposed in left lateral view in the counterslab (Figure 4D), traces along the dorsal and ventral margin of the pygostyle are interpreted as the *mm. levator caudae* and *depressor caudae*. These muscles flex the tail dorsally and ventrally; a well-developed *levator* muscle was previously hypothesized present in enantiornithines based on pygostyle morphology (Wang and O'Connor, 2017).

Gastroliths

A large, tight cluster of stones, measuring approximately 18.7 mm long and 9.9 mm at its widest point, is preserved in the counterslab directly adjacent to the left lateral margin of the cervical vertebrae and extending from the third to eighth vertebra (Figure 5). The stones form a tight oval mass that also includes flecks of carbonized organic matter. Based on their close association with the body of the bird, these stones are interpreted as gastroliths [gastrolith - "a hard object of no caloric value which is, or was, retained in the digestive tract of an animal, "sensu Wings (2007)]. The gastroliths visible in the surface are rounded, subspherical, small, and subequal in size, most with a long axis measuring around 0.52-0.72 mm. Although the gastroliths are still embedded in matrix (see below), some stones on the surface of the aggregate are visibly exposed and appear to be quartz. CT scans reveal that internally the mass consists of both large and small stones that vary from subangular to subrounded (Table 3). Noticeable gaps exist between the stones in some areas and other regions are high-density, both features also visible in CT scans of gastric mills preserved in *Archaeorhynchus* (Liu et al., 2023) (Figure 5). However, density contrast (as inferred by variation in grey value, reflective of relative density) between the gastroliths and matrix in STM7-156 appears to be lower than observed between gizzard stones (a specific type of gastrolith that is inferred to aid in digestion together with the presence of a muscular gizzard, together forming a gastric mill) preserved in specimens of the Jehol ornithuromorphs *Archaeorhynchus* and *Iteravis* (Liu et al., 2023). In addition, the total gastrolith volume in ornithuromorphs *Archaeorhynchus* and *Iteravis* is much smaller than the total volume observed in STM7-156 despite the much larger body size of these taxa (Liu et al., 2023) (Table 3). The number of individual gastroliths in STM7-156 is also proportionately higher than observed in these taxa, exceeding the number documented in all previously sampled specimens, including an anomalous specimen of *Archaeorhynchus*, in which the numerous gastroliths are all very small, most likely indicating they would shortly be passed and replaced (Liu et al., 2023). The two largest individual gastroliths in STM7-156 have a volume of 9.36 and 6.23 mm. Gastroliths of this size are very rare in the four sampled specimens of the larger *Archaeorhynchus* although similarly sized and larger gastroliths are present in the larger *Iteravis* (Liu et al., 2023). Together, this data indicates the gastroliths in STM7-156 do not represent a gastric mill (i.e., they are not gizzard stones), consistent with the position of the gastroliths in the esophagus and not within the abdominal cavity.

The soft tissue of the neck visible under UVA light does not surround the mass, rather the mass appears to overlie the fluorescing soft tissues on the left margin of the neck (Figure 4B). While it is possible that this mass of gastroliths belonged to another larger organism and was moved into contact with STM7-156 by currents, the intimate association between this gastrolith mass and the bird (in contact with the cervical vertebrae), the in situ preservation of the neck feathers, and the partial preservation of body soft tissues indicate limited post mortem disturbance of the carcass by strong currents and support the interpretation that the gastroliths belonged to this bird.

XRF analysis

Data was collected from three regions of the mudstone sediment matrix and three from the surface of the mass of gastroliths (Appendix 1). Because the gastroliths are not prepared, we were seeking to determine if the gastrolith matrix in which the gastroliths are embedded is chemically distinct from the matrix, potentially preserving chemical indicators of diet. The XRF data reveals high concentrations of Si, Al, and K, indicating both the sediment matrix and gastrolith matrix consists primarily of silica (SiO_2) and aluminum (Al_2O_3) and

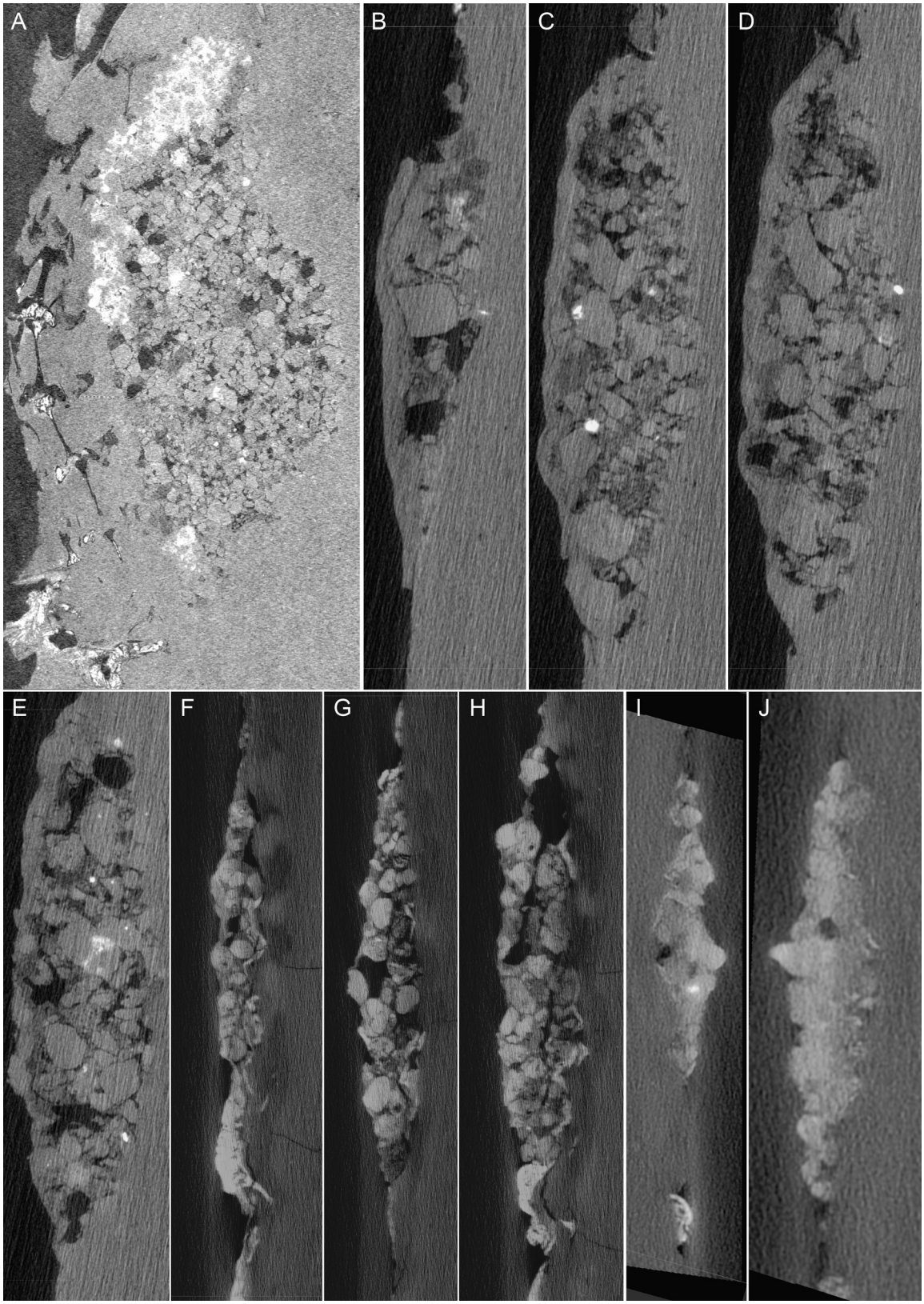

FIGURE 5. Computed tomography slices showing the cross-sectional morphology of Jehol bird gastrolith masses revealing internal spaces, high density regions, and the size and angularity of individual gastroliths. A-E, STM7-156; F-H, *Archaeorhynchus* IVPP V17075; I-J, *Archaeorhynchus* IVPP V17091.

TABLE 3. Comparison of the size of individual gastroliths and total gastrolith mass in *Chromeornis* STM7-156 with Jehol ornithuromorphs, *Archaeorhynchus* and *Iteravis*. Volumes are in mm^3. Asterix indicates estimates. Ranges for *Archaeorhynchus* and *Iteravis* taken from Liu et al. (2023). < indicates greater than that number of gastroliths (too many small low density objects to get a precise count).

Taxon	Collection No.	Body mass	Gastrolith No.	Average stone volume	Gastrolith volume range	Total gastrolith volume	Reference
Chromeornis	STM7-156	33.5	>800	1.09	<0.1-9.36	2454.6	current paper
Archaeorhynchus	IVPP V14287	261.83	47	2.14	<1-<8	100.76	Liu et al., 2023
Archaeorhynchus	IVPP V17091	250.93	94	2.59	<1-<7	243.36	Liu et al., 2023
Archaeorhynchus	IVPP V17075	201.65	321	0.67	<1-<3	214.65	Liu et al., 2023
Archaeorhynchus	IVPP V20312	486.83	75	1.92	<1-<10	144.03	Liu et al., 2023
Iteravis	IVPP V23346	349.21	12	29.42	<1-<90	353.01	Liu et al., 2023
Iteravis	IVPP V18958	208.2	15	16.33	<1-<60	244.93	Liu et al., 2023
Iteravis	IVPP V20133	297.68	17	11.06	<1-<40	188.05	Liu et al., 2023
Iteravis	IVPP V20134	233.79	45	10.8	<1-30	485.83	Liu et al., 2023

potassium (K_2O) oxides forming clay minerals (Chang et al., 2003). However, principle component (PC) analysis and discriminant analysis support that the composition of the sediment matrix is chemically different from the gastrolith matrix. When PC1 (56.7% of variance) is plotted against PC2 (27.7% of the variance), the gastrolith matrix data points cluster together and separate from the matrix indicating some compositional difference in the gastrolith matrix compared to that of the sediment (Figure 6). However, the gastrolith matrix varies along PC3 (7.2% of the matrix). Low PC1 values indicate relative increases in Cr, Pb, and Cu concentrations whereas high PC2 values indicate increases in Cr, Pb, Cu, and P concentrations. Similarly, low PC3 values additionally suggest relative increased concentrations in the elements Pb, Cr, Cu, Co, and S. Overall, the gastrolith matrix tends to differ from the surrounding sediment matrix in their increased concentrations of Cr, Pb, Cu, and possibly Co, S, and P. The chemical differences between the gastrolith matrix and sediment matrix strongly suggests that these stones did not naturally accumulate against the carcass.

Cladistic Analysis

We added STM7-156 to the Shen et al. *Neobohaiornis* matrix (Shen et al., 2024). Scorings were corrected for three characters across most taxa (Appendix 2): 86 (sternum ossification as two plates, a single flat element, a single element with a slight midline ridge, and a single element with a strongly projecting carina; the state with a slight midline ridge is meant to refer to taxa like *Con-*

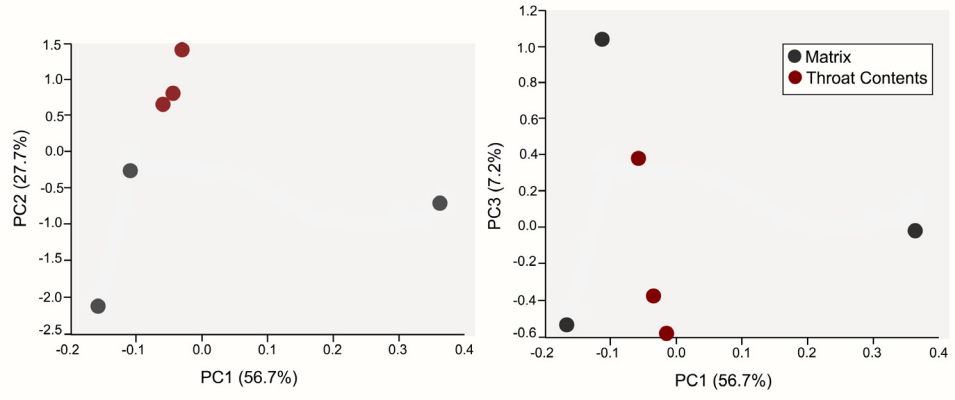

FIGURE 6.
Principle component analysis of x-ray fluorescence data taken from the surface of the gastrolith mass (gastrolith matrix) and the sediment matrix indicating that these two sample types are chemically distinct. Analysis indicates the

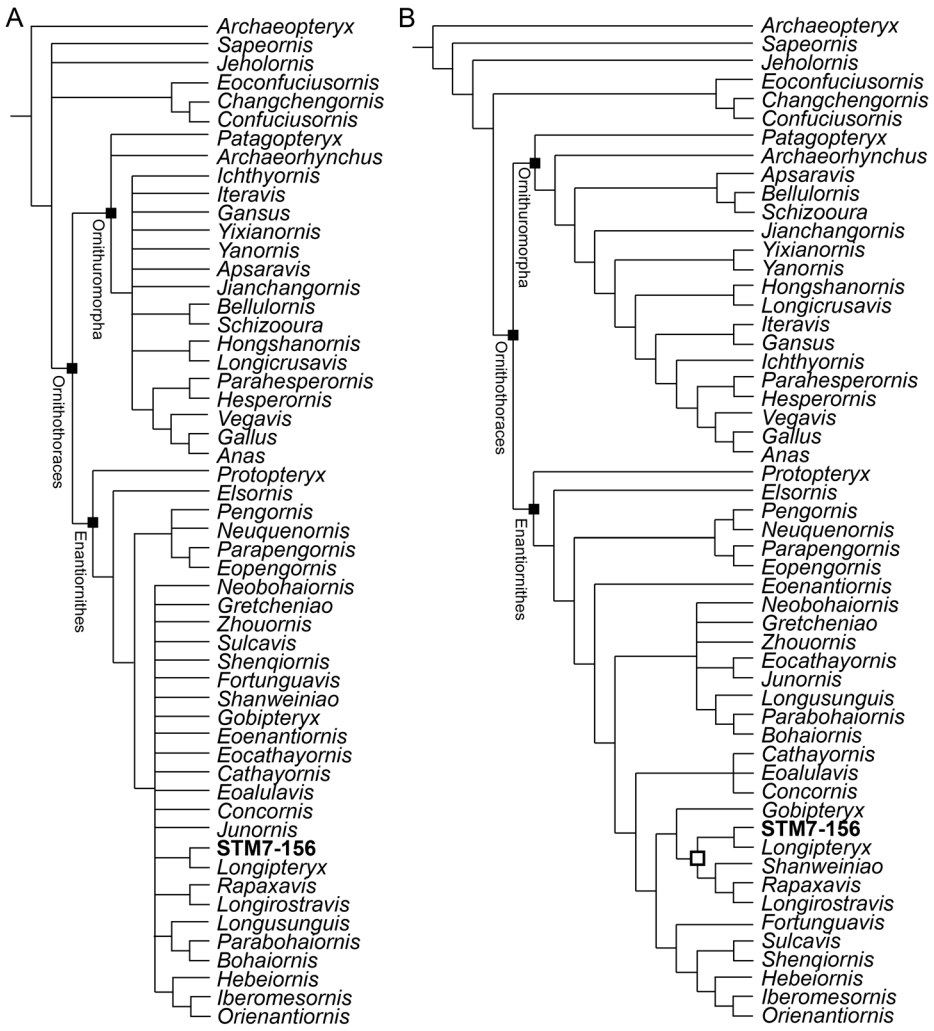

FIGURE 7. Cladogram depicting the hypothetical phylogenetic relationships of *Chromeornis* STM7-156 based on cladistic analysis. A, reduced consensus of 485 trees with *Vorona* removed in which most of Enantiornithes consists of a polytomy in which *Longipteryx* and *Chromeornis* STM7-156 form a clade; B, 50% majority rule tree in which Longipterygidae is resolved into two subclades: the Longipteryginae, consisting of *Longipteryx* and *Chromeornis* STM7-156, and the Longirostravinae, consisting of *Longirostravis, Shanweiniao,* and *Rapaxavis*.

fuciusornis whereas the sternal keel in enantiornithines is considered strongly projecting; the sternal keel is often lost due to poor preservation and it is best to score uncertainty in these instances); 99 (proximal margin of humerus concave in its central portion, rising ventrally and dorsally); and 140 (intermetacarpal space reaching the distal end of the alular metacarpal or terminating distal to the alular metacarpal). Character 99 was first used by Chiappe (Chiappe, 2002), in which it is only scored present in enantiornithines, indicating it must refer to the unique profile of the enantiornithine humerus, often referred to as 'saddle shaped.' However, more accurately, the humeral head is convex (not concave), separated from the dorsal and ventral tubercles by concavities. Therefore, this character is modified to read "proximal margin of humerus convex in its central portion" (see Supplemental Information). This morphology varies from weakly to strongly developed but is present in all but the most basal enantiornithines (pengornithids, *Protopteryx*).

The final matrix consists of 55 operational taxonomic units scored across 212 characters (Appendix 3). The matrix was analyzed in TNT (Goloboff et al., 2008) with the following parameters: memory set to 10,000 trees; traditional heuristic search using tree bisection reconnection (TBR) retaining one tree out of every 1,000 followed by a second round of TBR using saved trees. The first

round of TBR produced 5 trees 955 steps long. The second round of TBR recovered 486 trees the same length. The strict consensus of the first 5 trees indicated that *Vorona* was problematic due to its fragmentary nature, being recovered in an unusual phylogenetic position in a polytomy with *Jeholornis* and basal pygostylians (*Sapeornis*, Confuciusornithiformes). We removed *Vorona* in the reduced consensus tree of the 486 recovered trees (Figure 7A). This grouped *Longipteryx* with STM7-156 (supported by 9 characters; see Supplemental Information) and *Longirostravis* with *Rapaxavis* (supported by 10 characters) in a polytomy with other enantiornithines. The 50% majority rule tree recovered a monophyletic Longipterygidae (supported by 3 characters) with *Longipteryx* and STM7-156 forming the Longipteryginae (supported by 3 characters) in a sister clade relationship to the Longirostravinae (supported by a single character) formed by *Shanweiniao* as outgroup to *Rapaxavis* and *Longirostravis* (supported by 3 characters) (Figure 7B). The three characters that consistently support the relationship between *Longipteryx* and STM 7-156 in both the strict consensus and majority rule tree are: 26(0), dentary teeth present; 95(0), sternal pneumatic formina absent (a condition present in all known enantiornithines); 201(0), trochlea of metatarsals III and IV ending at the same level, which is coded as missing data in STM7-156 (for additional character support, see Supplemental Information).

DISCUSSION

The new taxon *Chromeornis funkyi*, represented by a nearly complete individual preserved in a slab and counterslab, increases the diversity of longipterygids and elucidates evolutionary trajectories within this distinctive clade. Exceptional traces provide a rare glimpse of soft tissues structures, improving our understanding of the postpatagium and m. *tibialis cranialis*, and confirming the absence of rectricial bulbs in enantiornithines. The unusual mass of gastroliths preserved within the esophagus represent a conundrum that cannot be resolved with currently available data but poses interesting questions about behavior and the evolution of the digestive system in enantiornithines to be explored in the future.

Longipterygid evolution

STM7-156 represents one of the smallest longipterygids uncovered thus far. Compared to other enantiornithines, longipterygids have three unique and distinctive characteristics: their elongate rostra, proportionately elongate premaxillary corpus, and rostrally restricted dentition (O'Connor et al., 2009; Zhang et al., 2001). These features are easily identifiable in STM7-156. Within the Longipterygidae there are significant differences with regards to body size, limb proportions, dental morphology, and the structure of the manus. *Longipteryx* (Longipteryginae) is the largest taxon with double the humeral length of small longirostravines and an estimated body mass of 100-155g compared to 38g in *Shanweiniao*, 44g in *Rapaxavis* and 42.6g in *Longirostravis* (Liu et al., 2012) (Table 2). Assessment of body size in *Boluochia* is prevented by poor preservation but it appears to be only slightly smaller than *Longipteryx* (O'Connor et al., 2011a).

Longipteryx, meaning 'long wing' in Latin, has the proportionately longest wings of any known Early Cretaceous enantiornithine (Zhang et al., 2001). It has an intermembral index between 1.44-1.51, compared to 1.07-1.23 in longirostravines (Table 2). With an intermembral index of 1.14 and a mass of 33.5g, *Chromeornis* is similar in body size and proportions to longirostravines. However, it shares several morphologies with *Longipteryx*. Teeth are proportionately large and recurved in *Longipteryx*, but smaller and appear peg-like in longirostravines. Although tooth shape is obscured by small size and poor preservation in most longirostravines, the teeth in *Chromeornis* appear to be more like those in *Longipteryx* with regards to proportionate size (crown height approaches the depth of the dentary) and shape (basally elongate, sharply tapered, strongly recurved). Whether the teeth were also crenulated with hypertrophied enamel cannot be determined, as the teeth are poorly preserved primarily as voids in STM7-156 (Figure 3B).

Longipteryx has large manual claws, whereas these are absent in longirostravines, a morphology that does not occur in other known Early Cretaceous enantiornithines. Manual claws are present in *Chromeornis* but proportionately smaller than those in *Longipteryx*. Cladistic analysis confirms the phylogenetic position of *Chromeornis* as a longipterygid and places it in the Longipteryginae indicating it is more closely related to *Longipteryx* than to longirostravines. This information suggests that longipterygids were ancestrally small bodied with intermembral indices ~1.1, as is typical of Early Cretaceous enantiornithines. Limited data suggests that in the Longipteryginae lineage body size and proportionate wing length increased, whereas in the Longirostravinae the manus reduced in

length and manual unguals were lost, a trend that parallels ornithurine birds.

Unusual gastrolith mass

STM7-156 preserves a large mass of gastroliths in very close association with the neck (in contact with the cervical vertebrae) (Figures 1-3). Here we use the definition of gastrolith sensu Wings that a gastrolith is “a hard object of no caloric value which is, or was, retained in the digestive tract of an animal” (Wings, 2007). The most straight forward interpretation is that this mass represents a cranially displaced gastric mill and that these gastroliths are gizzard stones. However, a definitive gastric mill has not been previously identified in the dozens of enantiornithine specimens formally described from Jehol deposits, with hundreds of specimens examined (O’Connor, 2019). Gastroliths were reported in a specimen of the bohaiornithid enantiornithine *Bohaiornis* but due to their small number they were not interpreted as gizzard stones but as rangle (a small number of stones ingested by predatory birds to help clean the digestive tract) (Li et al., 2014). However, these traces were later demonstrated to represent some silicified soft tissue (Liu et al., 2021), probably adipocere (O’Connor, 2025). Due to this lack of evidence, it has been suggested that a gastric mill was absent in enantiornithines and even invoked as a possible factor in their extinction alongside non-avian dinosaurs (O’Connor, 2019). However, the complete absence of a gastric mill in enantiornithines is at odds with the known phylogenetic distribution of this feature, present in stem-ward lineages (*Jeholornis, Sapeornis,* Jinguofortisidae) and ornithuromorphs (7 out of 25 Jehol genera are documented with gastroliths) (O’Connor and Zhou, 2019; O’Connor, 2019).

The mass in STM7-156 differs from previously identified gastroliths identified as gizzard stones (part of a gastric mill) in the position of the gastroliths, in the esophagus and not the ventriculus, and the shape of the mass, being oval (elongated parallel to the neck). Among Jehol birds, the gastric mill is typically preserved in situ within the abdominal cavity, as in nearly every articulated or near articulated specimen of ornithuromorph preserving gizzard stones (Liu et al., 2023). In ornithuromorphs in which the mass is tightly packed (all articulated specimens of *Archaeorhynchus*; the fewer but larger gastroliths in *Iteravis* form a loose cluster) the gastroliths form a rounded mass (Liu et al., 2023). The difference in shape is likely a product of the position in which the gastroliths are preserved, with the long and oval shape of the mass in STM7-156 a product of the elongated esophagus, whereas the ventriculus is more spherical. Only in *Jeholornis* is the gastric mill sometimes preserved outside the abdominal cavity; in these specimens the mass is preserved a short distance from the body presumably due to postmortem rupture of the ventriculus and abdomen (O'Connor et al., 2018). A complete gastric mill associated with an isolated sternum of *Gansus* has been reported from the Xiagou Formation, where only disarticulated avian remains have been recovered (Wang et al., 2016). No previous specimen preserves the gastroliths in the esophagus as observed in STM7-156. However, it is possible that the gastrolith mass moved into the esophagus post-mortem. Upon death, the sphincter between the proventriculus and esophagus loosens; compression of the carcass, as in burial, could potentially allow the gastric mill to move from the ventriculus into the esophagus. This is more likely to occur when a carcass is disturbed, as suggested by the disarticulation of the right wing in STM7-156.

However, comparison with CT data of gizzard stones preserved in sympatric ornithuromorphs indicates that the mass in STM7-156 does not represent a gastric mill. Published CT data is available for two taxa, *Archaeorhynchus* and *Iteravis* (Liu et al., 2023). Both species are much larger than *Chromeornis* – even the smallest known individuals of these taxa are more than 6 times the estimated body mass of STM7-156 (Table 3). Despite this, the gastrolith volume in *Chromeornis* ranges from 5 to 24 times the size of the smallest and largest gastric mills recovered from these taxa. While the number of gastroliths cannot be precisely quantified in STM7-156 due to the quality of the CT scan data and the poor contrast between the gastroliths and the matrix, our approximation suggests that the number of gastroliths is also far higher than that ingested by these taxa (Liu et al., 2023). The mass in STM7-156 also includes stones that are disproportionately large for its body size. Although the lithology of the gastroliths in STM7-156 is unknown, and indeed not reported for other Cretaceous dinosaur gizzard stones, the density contrast between the gastroliths and matrix appears to be less pronounced than observed between the matrix and gizzard stones in specimens of *Iteravis* and *Archaeorhynchus* (Figure 5). This evidence, together with the proportionate size of both individual gastroliths and the entire gastrolith mass and the preserved location in the esophagus in *Chromeornis* STM7-156, is inconsistent with the inter-

pretation that these stones had a digestive function. This data supports interpretations that a gastric mill was absent in Enantiornithes (O'Connor, 2019).

If not a gizzard, what these gastroliths signify is a puzzle. Birds ingest and expel stones for various reasons. Predatorial birds do so to cleanse the cranial portions of the digestive tract and accidentally ingested stones are also egested in nests prior to feeding young (Wings, 2007). This also occurs in penguins, although the stones are most likely ingested intentionally as ballasts consistent with their subaqueous foraging habits and given that other volant piscivorous birds do not intentionally ingest stones for digestive purposes. Birds also intentionally ingest grit for nutritional purposes, ingesting calcium rich rocks to add in eggshell production (Wings, 2007), or medicinal purposes, such as the removal of parasites (Robinson et al., 2008). However, none of these hypotheses is consist with the large number of gastroliths forming the mass in STM7-156.

Alternative interpretations for the presence of this gastrolith mass are weakened by the uniqueness of this trace. Although ingested food remains are regularly observed in the esophageal crop of Jehol birds like *Sapeornis* and *Yanornis* (Zheng et al., 2011; Zheng et al., 2014), to our knowledge this is the first report of significant gastroliths in the esophagus of any fossil animal. In living birds, only very small amounts of grit are reported in the esophagus (Bartonek, 1969). We tentatively speculate that the ingested stones are pathological – the product of abnormal behavior, perhaps due to illness. The mass may have been in the process of being regurgitated at the time of death and possibly the cause of death itself (the large size of the mass relative to its body may have caused the bird to asphyxiate). With only a single enantiornithine specimen, more data is required to understand the significance of the gastrolith mass in STM7-156. In the future, searching for gastrolith masses near but not necessarily intrabdominal or in situ in enantiornithines may provide additional evidence that may elucidate the role of gastroliths in the biology of this clade.

The absence of a gastric mill in enantiornithines

A gastric mill is not preserved in any of the many recovered nearly complete and articulated specimens collected from Lower Cretaceous Lagerstätten, nor the partial but three-dimensionally preserved specimens recovered from Upper Cretaceous deposits (e.g., *Elsornis, Navaornis, Neuquenornis, Yuornis*) (Chiappe and Calvo, 1994; Chiappe et al., 2024; Chiappe et al., 2006; Xu et al., 2021). While the presence of a gastric mill correlates with tooth loss in ornithuromorphs, this feature is absent even in toothless enantiornithines (Wang et al., 2024). This may suggest that enantiornithines did not evolve diets relying on gizzard stones for digestion (as previously suggested, enantiornithines may have primarily fed on soft foods not requiring the aid of a gastric mill) (O'Connor, 2019), or that enantiornithines evolved alternative solutions for digesting these hard foods, such as soft tissue adaptations unlikely to fossilize.

We suggest that this difference with other avian lineages may at least partially reflect enantiornithine aerial abilities. The morphology of the pectoral girdle and proportionately small sternum of enantiornithines indicates limited flight capabilities compared to ornithuromorphs (O'Connor, 2022). Notably, the absence of a globe-shaped humeral head and fully closed triosseal canal to stabilize the m. *supracoracoideus* ligament suggest that the forelimbs would have had a narrower range of motion compared to ornithuromorphs, limiting enantiornithines to intermittent flight styles or brief continuous flapping (consistent with predictions for Early Cretaceous members of this clade) (Chiappe et al., 2019; Serrano et al., 2018) and suggesting comparatively weaker ground take off capabilities and limited migratory abilities compared to ornithuromorphs. This implies that, compared to ornithuromorphs, the added weight of gastroliths for extended periods of time, as in a gastric mill, would have had a more detrimental impact on enantiornithine flight. This also strongly suggests that the unusually large size of the gastrolith mass in STM7-156 is not due to unique properties of the enantiornithine gastric mill. The size of the gastric mill is proportionately larger in non-avian dinosaurs than it is in the Early Cretaceous ornithuromorphs *Iteravis* and *Archaeorhynchus*; it is hypothesized that the smaller size in early birds is due to constraints imposed by the evolutionary appearance of flight (Liu et al., 2023). The limited flight capabilities of enantiornithines compared to ornithuromorphs suggests that, if a gastric mill was present, it would be smaller, not larger in enantiornithines.

Ingesting gastroliths also requires significant time spent on the ground collecting stones of the right size and lithology. Although this could be combined with foraging in terrestrial taxa, such as the ornithuromorph *Archaeorhynchus*, known Early

Cretaceous enantiornithines exclusively utilized arboreal habits (O'Connor, 2022). Considering evidence that suggests ground-take off may have been physically demanding for enantiornithines, these birds would theoretically incur greater energetic costs when moving between the ground and their arboreal habits. Notably, the basal pygostylian *Sapeornis*, with its very primitive pectoral girdle (ossified sternum absent, plesiomorphic axe-shaped scapulocoracoid) (Zhou and Zhang, 2003) and thus hypothetically limited flight capabilities (possibly limited to soaring) (Serrano and Chiappe, 2017), has a proportionately small gastric mill, typically consisting of only a few large stones (Zheng et al., 2011). The unusually small gastric mill in *Sapeornis* and the complete absence of this structure in enantiornithines may reflect a cost-benefit balance between increased digestive capabilities, the energetic cost of foraging for stones, and decreased flight functionality in stem-avian lineages, which lack the full suite of skeletal adaptations for advanced flight capabilities observed in ornithuromorphs (Lowi-Merri et al., 2025; O'Connor, 2022).

CONCLUSIONS

We describe *Chromeornis funkyi* from STM7-156, a new species of longipterygid enantiornithine with the proportionately elongate rostrum and distally restricted dentition that characterizes this unique clade. The new taxon is similar in size and proportions to previously described longirostravines but otherwise resembles *Longipteryx* in having large, recurved teeth, manual claws, and simple sternal lateral trabeculae. Cladistic analysis resolves this new species as a longipterygine more closely related to *Longipteryx* than to other longipterygids suggesting the ancestral longipterygid was small (~40 g), with forelimbs only slightly longer than the hindlimbs, and large manual claws. STM7-156 preserves a large mass of gastroliths adjacent to the neck and presumably within the esophagus. Comparison with ornithuromorphs indicates that these gastroliths do not represent a gastric mill. The significance of this trace is unknown. We suggest the absence of a gastric mill in enantiornithines reflects their relatively limited flight capabilities. We are grateful to Paul and Sheila Demkovich for their support of paleontological research at the FMNH.

ACKNOWLEDGMENTS

This work was supported by grants from National Natural Science Foundation of China (42288201 and 41402017), Shandong Provincial Natural Science Foundation (ZR2020MD026 and Ts20190954). We thank Xiaomei Zhang, Xuwei Yin, and Shiying Yin for facilitating our visit to the STM. We thank Shannon Hackett and John Bates (FMNH) for their valuable input with regards to avian gastroliths, and Laure Dussubieux and the Elemental Analysis Facility (FMNH) for use of the XRF device.

REFERENCES

Bartonek, J.C. 1969. Build-up of grit in three pochard species in Manitoba. *Willson Bulletin*, 81:96-97.

Baumel, J.J., and Witmer, L.M. 1993. Osteologia; pp. 45-132 *i*n J. J. Baumel, A. S. King, J. E. Breazile, H. E. Evans, and J. C. Vanden Berge (eds.), Handbook of Avian Anatomy: Nomina Anatomica Avium, Second Edition. Nuttall Ornithological Club, Cambridge.

Chang, M.-M., Chen, P.-J., Wang, Y.-Q., Wang, Y., and Miao, D.-S. eds (2003) The Jehol Fossils: The Emergence of Feathered Dinosaurs, Beaked Birds and Flowering Plants. Shanghai Scientific & Technical Publishers, Shanghai.

Chen, R.-S., Wang, M., Dong, L.-P., Zhou, G.-W., Xu, X., Deng, K., Xu, L.-M., Zhang, C., Wang, L.-C., Du, H.-G., Lin, G.-M., Lin, M., and Zhou, Z.-H. 2025. Earliest short-tailed bird from the Late Jurassic of China. Nature, 638:441-448.

Chiappe, L.M. 2002. Basal bird phylogeny: problems and solutions; pp. 448-472 *i*n L. M. Chiappe, and L. M. Witmer (eds.), Mesozoic Birds: Above the Heads of Dinosaurs. University of California Press, Berkeley.

Chiappe, L.M., and Calvo, J.O. 1994. *Neuquenornis volans*, a new Late Cretaceous bird (Enantiornithes: Avisauridae) from Patagonia, Argentina. Journal of Vertebrate Paleontology, 14:230-246.

Chiappe, L.M., Meng, Q.-J., Serrano, F.J., Sigurdsen, T., Wang, M., Bell, A., and Liu, D. 2019. New *Bohaiornis*-like bird from the Cretaceous of China: enantiornithine interrelationships and flight performance. PeerJ, 7:1-50.

Chiappe, L.M., Navalón, G., Martinelli, A.G., Carvalho, I.D.S., Miloni Satucci, R., Wu, Y.-H., and Field, D.J. 2024. Cretaceous bird from Brazil informs the evolution of the avian skull and brain. Nature, 635:376-381.

Chiappe, L.M., Suzuki, S., Dyke, G.J., Watabe, M., Tsogtbaatar, K., and Barsbold, R. 2006. A new enantiornithine bird from the Late Cretaceous of the Gobi Desert. Journal of Systematic Palaeontology, 5:193-208. https://doi.org/10.1017/S1477201906001969

Chiappe, L.M., and Walker, C.A. 2002. Skeletal morphology and systematics of the Cretaceous Euenantiornithes (Ornithothoraces: Enantiornithes); pp. 240-267 *i*n L. M. Chiappe, and L. M. Witmer (eds.), Mesozoic Birds: Above the Heads of Dinosaurs. University of California Press, Berkeley.

Clark, A.D., Atterholt, J.A., Scanella, J.B., Carroll, N., and O'Connor, J.K. 2024. New enantiornithine diversity in the Hell Creek Formation and the functional morphology of the avisaurid tarsometatarsus. PLoS ONE, 19:1-25.

Clark, A.D., Hu, H., Benson, R.B.J., and O'Connor, J.K. 2023. Reconstructing the dietary habits and trophic positions of the Longipterygidae (Aves: Enantiornithes) using neontological and comparative morphological methods. PeerJ, 11:1-32.

Goloboff, P.A., Farris, J.S., and Nixon, K.C. 2008. TNT, a free program for phylogenetic analysis. Cladistics, 24:774-786. https://doi.org/10.1111/j.1096-0031.2008.00217.x

Hopson, J.A. 2001. Ecomorphology of avian and nonavian theropod phalangeal proportions: implications for the arboreal versus terrestrial origin of bird flight; pp. 211-235 *i*n J. Gauthier, and L. F. Gall (eds.), New Perspectives on the Origin and Early Evolution of Birds. Peabody Museum of Natural History, New Haven.

Hou, L., Chiappe, L.M., Zhang, F., and Chuong, C.-M. 2004. New Early Cretaceous fossil from China documents a novel trophic specialization for Mesozoic birds. Naturwissenschaften, 91:22-25.

Hu, H., and O'Connor, J.K. 2017. First species of Enantiornithes from Sihedang elucidates skeletal development in Early Cretaceous enantiornithines. Journal of Systematic Palaeontology, 15:909-926.

Li, L., Gong, E.-P., Zhang, L.-D., Yang, Y.-J., and Hou, L.-H. 2010. A new enantiornithine bird (Aves) from the Early Cretaceous of Liaoning, China. Acta Palaeontologica Sinica, 49:524-531.

Li, L., Wang, J.-Q., Zhang, X., and Hou, S.-L. 2012. A new enantiornithine bird from the Lower Cretaceous Jiufotang Formation in Jinzhou area, Western Liaoning Province, China. Acta Geologica Sinica, 86:1039-1044.

Li, Z.-H., Wang, C.-C., Wang, M., Chiang, C.-C., Wang, Y., Zheng, X.-T., Huang, E.-W., Hsiao, K., and Zhou, Z.-H. 2020. Ultramicrostructural reductions in teeth: implications for dietary transition from non-avian dinosaurs to birds. BMC Evolutionary Biology, 20:1-8.

Li, Z.-H., Zhou, Z.-H., Wang, M., and Clarke, J.A. 2014. A new specimen of large-bodied basal enantiornithine *Bohaiornis* from the Early Cretaceous of China and the inference of feeding ecology in Mesozoic birds. Journal of Paleontology, 88:99-108.

Liu, D., Chiappe, L.M., Zhang, Y.-G., Serrano, F.J., and Meng, Q.-J. 2019. Soft tissue preservation in two new enantiornithine specimens (Aves) from the Lower Cretaceous Huajiying Formation of Hebei Province, China. Cretaceous Research, 95:191-207. https://doi.org/10.1016/j.cretres.2018.10.017

Liu, D., Zhou, Z.-H., and Zhang, Y.-G. 2012. Mass estimate and evolutionary trend in Chinese Mesozoic fossil birds. Vertebrata Palasiatica, 50:39-52.

Liu, S.-M., Li, Z.-H., Bailleul, A.M., Wang, M., and O'Connor, J.K. 2021. Investigating possible gastroliths in a referred specimen of *Bohaiornis guoi* (Aves: Enantiornithes). Frontiers in Earth Science, 9:1-13. https://doi.org/10.3389/feart.2021.635727

Liu, S.-M., Li, Z.-H., Liu, D., and O'Connor, J.K. 2023. Quantifying the gastral mass in Early Cretaceous ornithuromorphs (Aves, Ornithothoraces) from the Jehol avifauna. Palaeontology, 66:1-17.

Lowi-Merri, T.M., Hu, H., O'Connor, J.K., Benson, R.B.J., Claramont, S., and Evans, D.C. 2025. Enlargement of sternum traits facilitated the evolution of powered flight in birds. Nature Ecology & Evolution:1-14.

Martin, L.D., and Lim, J.-D. 2005. Soft body impression of the hand in *Archaeopteryx*. Current Science, 89:1089-1090.

Miller, C.V., Pittman, M., Wang, M., Zheng, X.-T., and Bright, J.A. 2022. Diet of Mesozoic toothed birds (Longipterygidae) inferred from quantitative analysis of extant avian diet proxies. BMC Biology, 20:1-37.

Morschhauser, E., Varricchio, D.J., Gao, C.-H., Liu, J.-Y., Wang, X.-R., Cheng, X.-D., and Meng, Q.-J. 2009. Anatomy of the Early Cretaceous bird *Rapaxavis pani*, a new species from Liaoning Province, China. Journal of Vertebrate Paleontology, 29:545-554.

Navalón, G., Marugán-Lobón, J., Chiappe, L.M., Sanz, J.L., and Buscalioni, A.D. 2015. Soft-tissue and dermal arrangement in the wing of an Early Cretaceous bird: Implications for the evolution of avian flight. Scientific Reports, 5:14864.

O'Connor, J., and Chiappe, L.M. 2011. A revision of enantiornithine (Aves: Ornithothoraces) skull morphology Journal of Systematic Palaeontology, 9:135-157.

O'Connor, J., Falk, A.R., Wang, M., and Zheng, X.-T. 2020. First report of immature feathers in juvenile enantiornithines from the Early Cretaceous Jehol avifauna. Vertebrata Palasiatica, 58:24-44.

O'Connor, J., and Zhou, Z.-H. 2019. The evolution of the modern avian digestive system – insights from paravian fossils from the Yanliao and Jehol biotas. Palaeontology, 63:13-27.

O'Connor, J., Zhou, Z.-H., and Zhang, F.-C. 2011a. A reappraisal of *Boluochia zhengi* (Aves: Enantiornithes) and a discussion of intraclade diversity in the Jehol avifauna, China. Journal of Systematic Palaeontology, 9:51-63.

O'Connor, J.K. 2019. The trophic habits of early birds. Palaeogeography, Palaeoclimatology, Palaeoecology, 513:178-195. https://doi.org/10.1016/j.palaeo.2018.03.006

O'Connor, J.K. 2022. Primer: Enantiornithes. Current Biology, 32:R1042-R1072.

O'Connor, J.K. 2025. Insights into the early evolution of modern avian physiology from fossilized soft tissues from the Mesozoic. Philosophical Transactions of the Royal Society of London B Biological Sciences, 380:1-12.

O'Connor, J.K., Atterholt, J.A., Bailleul, A.M., Wang, M., Kuo, P.-C., and Zhou, Z.-H. 2025a. Description and osteohistology of two early immature enantiornithines (Aves: Ornithothoraces) from the Early Cretaceous Jehol Biota. Geobios, 90:103-122.

O'Connor, J.K., Chiappe, L.M., and Bell, A. 2011b. Pre-modern birds: avian divergences in the Mesozoic; pp. 39–114 in G. D. Dyke, and G. Kaiser (eds.), Living Dinosaurs: the Evolutionary History of Birds. J. Wiley & Sons, Hoboken, NJ.

O'Connor, J.K., Chiappe, L.M., Gao, C.-H., and Zhao, B. 2011c. Anatomy of the Early Cretaceous enantiornithine bird *Rapaxavis pani*. Acta Palaeontologica Polonica, 56:463–475.

O'Connor, J.K., Clark, A.D., Herrera, F., Yang, X., Wang, X.-L., Zheng, X.-T., Hu, H., and Zhou, Z.-H. 2024. Direct evidence of frugivory in the Mesozoic bird Longipteryx contradicts morphological proxies for diet. Current Biology, 34:4559-4566.

O'Connor, J.K., Clark, A.D., Kuo, P.-C., Wang, M., Shinya, A., Van Beek, C., and Chang, H.-L. 2025b. Avian features of *Archaeopteryx* feeding apparatus reflect elevated demands of flight. The Innovation. https://doi.org/10.1016/j.xinn.2025.101086

O'Connor, J.K., Wang, X.-L., Sullivan, C., Wang, Y., Zheng, X.-T., Hu, H., Zhang, X.-M., and Zhou, Z.-H. 2018. First report of gastroliths in the Early Cretaceous basal bird *Jeholornis*. Cretaceous Research, 84:200-208.

O'Connor, J.K., Wang, X.-R., Chiappe, L.M., Gao, C.-H., Meng, Q.-J., Cheng, X.-D., and Liu, J.-Y. 2009. Phylogenetic support for a specialized clade of Cretaceous enantiornithine birds with information from a new species. Journal of Vertebrate Paleontology, 29:188-204.

O'Connor, J.K., Zheng, X.-T., Wang, X.-L., Zhang, X.-M., and Zhou, Z.-H. 2015. The gastral basket in basal birds and their close relatives: size and possible function. Vertebrata Palasiatica, 53:133-152.

Robinson, S.A., Forbes, M.R., and Herbert, C.E. 2008. Is the Ingestion of Small Stones by Double-Crested Cormorants a Self-Medication Behavior. The Condor, 110:782-785.

Serrano, F. J., and Chiappe, L. M. (2017). Aerodynamic modelling of a Cretaceous bird reveals thermal soaring capabilities during early avian evolution. Journal of the Royal Society Interface, 14(132), 20170182.

Serrano, F.J., Chiappe, L.M., Palmqvist, P., Figuerirido, B., Marugán-Lobón, J., and Sanz, J.L. 2018. Flight reconstruction of two European enantiornithines (Aves, Pygostylia) and the achievement of bounding flight in Early Cretaceous birds. Palaeontology, 61:359-368.

Shen, C.-Z., Clark, A.D., Fang, H., Chen, S.-K., Jiang, H.-X., Ji, Q., and O'Connor, J.K. 2024. A new diminutive species of bohaiornithid enantiornithine (Aves: Ornithothoraces) from the Lower Cretaceous Jehol Group, northern China. Scientific Reports, 14:1-15.

Stidham, T.A., and O'Connor, J.K. 2021. The evolutionary and functional implications of the unusual quadrate of *Longipteryx chaoyangensis* (Avialae: Enantiornithes) from the Cretaceous Jehol Biota of China. Journal of Anatomy, 239(5):1066-1074.

Tanaka, G., Zhou, B.-C., Zhang, Y.-F., Siveter, D.J., and Parker, G.A. 2017. Rods and cones in an enantiornithine bird eye from the Early Cretaceous Jehol Biota. Heliyon, 3:1-39.

Vanden Berge, J.C., and Zweers, G.A. 1993. Myologia; pp. 189-250 in J. J. Baumel, A. S. King, J. E. Breazile, H. E. Evans, and J. C. Vanden Berge (eds.), Handbook of Avian Anatomy: Nomina Anatomica Avium, Second Edition. Nuttall Ornithological Club, Cambridge.

Wang, M., O'Connor, J.K., Pan, Y.-H., and Zhou, Z.-H. 2017. A bizarre Early Cretaceous enantiornithine bird with unique crural feathers and an ornithuromorph plough-shaped pygostyle. Nature Communications, 8:1-12.

Wang, W., and O'Connor, J.K. 2017. Morphological coevolution of the pygostyle and tail feathers in Early Cretaceous birds. Vertebrata Palasiatica, 55:289-314.

Wang, X.-L., Clark, A.D., O'Connor, J.K., Zhang, X.-Y., Wang, X., Zheng, X.-T., and Zhou, Z.-H. 2024. First Edentulous Enantiornithine (Aves: Ornithothoraces) from the Early Cretaceous Jehol Avifauna. Cretaceous Research, 159:1-14.

Wang, X.-R., Zhao, B., Shen, C.-Z., Liu, S.-Z., Gao, C.-H., Cheng, X.-D., and Zhang, F.-J. 2015. New material of *Longipteryx* (Aves: Enantiornithes) from the Lower Cretaceous Yixian Formation of China with the first recognized avian tooth crenulations. Zootaxa, 3941:565-578.

Wang, Y.-M., O'Connor, J.K., Li, D.-Q., and You, H.-L. 2016. New information on postcranial skeleton of the Early Cretaceous *Gansus yumenensis* (Aves: Ornithuromorpha). Historical Biology, 28:666-679.
https://doi.org/10.1080/08912963.2015.1006217

Wings, O. 2007. A review of gastrolith function with implications for fossil vertebrates and a revised classification. Acta Palaeontologica Polonica, 52:1-16.

Xing, L.-D., Cockx, P., O'Connor, J.K., and McKellar, R.C. 2020. A newly discovered enantiornithine foot preserved in mid-Cretaceous Burmese amber. Palaeoentomology, 3:212-219.

Xu, L., Buffetaut, E., O'Connor, J.K., Zhang, X.-L., Jia, S.-H., Zhang, J.-M., Chang, H.-L., and Tong, H.-Y. 2021. A new, remarkably preserved, enantiornithine bird from the Upper Cretaceous Qiupa Formation of Henan (central China) and convergent evolution between enantiornithines and modern birds. Geological Magazine.

Yun, C.-G. 2019. Comments on the taxonomic validity of *Camptodontornis yangi* (Li, Gong, Zhang, Yang, and Hou, 2010) and its relationships to *Longipteryx chaoyangensis* Zhang, Zhou, Hou, and Gu, 2000 and *Boluochia zhengi* Zhou, 1995. Zootaxa, 4652:391-392.

Zhang, F., and Zhou, Z. 2000. A primitive enantiornithine bird and the origin of feathers. Science, 290:1955-1960.

Zhang, F., Zhou, Z., Hou, L., and Gu, G. 2000. Early diversification of birds: evidence from a new opposite bird. Kexue Tongbao, 45:2650-2657.

Zhang, F., Zhou, Z., Hou, L., and Gu, G. 2001. Early diversification of birds: evidence from a new opposite bird. Chinese Science Bulletin, 46:945-949.

Zheng, X.-T., Martin, L.D., Zhou, Z.-H., Burnham, D.A., Zhang, F.-C., and Miao, D. 2011. Fossil evidence of avian crops from the Early Cretaceous of China. Proceedings of the National Academy of Sciences, USA, 108:15904-15907.

Zheng, X.-T., O'Connor, J.K., Huchzermeyer, F.W., Wang, X.-L., Wang, Y., Zhang, X.-M., and Zhou, Z.-H. 2014. New specimens of *Yanornis* indicate a piscivorous diet and modern alimentary canal. PLoS ONE, 9:e95036.
https://doi.org/10.1371/journal.pone.0095036

Zheng, X.-T., O'Connor, J.K., Wang, X.-L., Pan, Y.-H., Wang, Y., Wang, M., and Zhou, Z.-H. 2017. Exceptional preservation of soft tissue in a new specimen of Eoconfuciusornis and its biological implications. National Science Review, 4:441-452. 10.1093/nsr/nwx004

Zheng, X.-T., Wang, X.-L., O'Connor, J.K., and Zhou, Z.-H. 2012. Insight into the early evolution of the avian sternum from juvenile enantiornithines. Nature Communications, 3:1-8. https://doi.org/10.1038/ncomms2104

Zhou, Z. 1995. Discovery of a new enantiornithine bird from the Early Cretaceous of Liaoning, China. Vertebrata Palasiatica, 33:99-113.

Zhou, Z., and Zhang, F. 2001. Two new ornithurine birds from the Early Cretaceous of western Liaoning, China. Chinese Science Bulletin, 46:1258-1264.

Zhou, Z., and Zhang, F. 2003. Anatomy of the primitive bird *Sapeornis chaoyangensis* from the Early Cretaceous of Liaoning, China. Canadian Journal of Earth Sciences, 40:731-747. https://doi.org/10.1139/E03-011

Zhou, Z.-H., and Wang, M. 2024. Cretaceous fossil birds from China. Geological Society London Special Publications, 544:SP544-2023.

APPENDICES

APPENDIX 1.

X-ray fluorescence data from the surface of the gastrolith mass (g1-g3) and the surrounding rock matrix (m1-m3) of STM7-156. Values are in parts per million (ppm). "<LOD" indicates that the value is lower than the point of detection.

Time	**1/18/2024 0:00**	**1/18/2024 3:45**	**1/18/2024 3:40**	**1/18/2024 3:36**	**1/18/2024 3:29**	**1/18/2024 3:25**
Units	ppm	ppm	ppm	ppm	ppm	ppm
SAMPLE	7-156 g3	7-156 m3	7-156 g2	7-156 g1	7-156 m2	7-156 m1
Mo	4.73	3.2	4.87	4	4.48	4.96
Mo Error	1.78	1.67	1.74	1.71	1.7	1.74
Zr	246.64	199.97	257.03	222.34	219.69	206.5
Zr Error	3.46	3.01	3.44	3.19	3.16	3.17
Y	97.51	71.89	128.34	69.54	72.09	63.51
Y Error	2.35	2.06	2.51	2.07	2.1	2.06
Sr	210.21	137.33	228.62	166.9	169.24	153.68
Sr Error	3.1	2.45	3.14	2.7	2.7	2.67
U	7.3	6.54	<LOD	<LOD	7.84	<LOD
U Error	3.75	3.57	5.41	5.47	3.78	5.52
Rb	111.99	112.79	110	117.23	128.48	114.82
Rb Error	1.78	1.75	1.74	1.78	1.84	1.8
Th	20.62	19.82	21.55	22.61	21.36	21.71
Th Error	2.34	2.21	2.31	2.33	2.29	2.34
Pb	30.88	21.5	34.55	31.82	24.94	18.52
Pb Error	3.26	2.83	3.28	3.2	2.96	2.83
As	7.39	<LOD	4.24	5.59	<LOD	4.57
As Error	2.76	3.46	2.7	2.66	3.62	2.38
Hg	<LOD	<LOD	<LOD	<LOD	6.05	8.49
Hg Error	5.17	5.16	5.06	5.05	3.37	3.6
Zn	67.54	50.38	65.53	59.37	57.8	59.62
Zn Error	5.44	4.86	5.25	5.1	5	5.24
Cu	43.21	24.58	46.4	32.3	30.38	25.01
Cu Error	8.25	7.76	8.1	7.82	7.72	7.96
Ni	15.58	13.21	25.49	25.87	26	27.53
Ni Error	8.02	7.85	7.97	7.96	7.9	8.28
Co	60.71	59.64	107.5	73.12	54.27	80.02
Co Error	27.06	25.3	27.09	26.17	27.38	30.91
Fe	5098.24	4699.24	5162.56	4940.68	5779.01	6972.62
Fe Error	69.03	64.09	67.58	66.13	70.72	80.02
Mn	169.83	127.95	154.68	133.25	157.12	195.67
Mn Error	27.09	25.16	26.08	25.63	25.82	27.71
Cr	40.19	40.45	51.28	48.93	31.33	26.85

Time	1/18/2024 0:00	1/18/2024 3:45	1/18/2024 3:40	1/18/2024 3:36	1/18/2024 3:29	1/18/2024 3:25
Cr Error	5.28	11.03	5.48	5.35	5.06	5.11
V	48.42	28.45	45.51	54.35	43.04	33.31
V Error	10.3	7.14	10.57	10.71	9.23	9.16
Ti	1736.86	1281.69	1889.02	2123.3	1803.87	1485.11
Ti Error	34.28	24.32	35.58	36.37	31.56	31.11
Ca	7284.72	3475.69	7736.96	6283.89	7248.14	18509.19
Ca Error	81.43	56.29	83.95	77.51	80.16	271.81
K	30189.62	29383.45	29347.22	29742.16	29675.2	27962.56
K Error	220.56	215.7	217.76	220.76	215.82	219.6
S	7124.07	4067.29	6879.33	6853.14	3580.2	35942.64
S Error	134.54	112.97	133.46	137.35	105.89	307.64
Ba	400.23	363.73	403.05	416.59	400.22	417.33
Ba Error	29.23	31.13	29.35	29.75	29.51	30.82
Sb Error	13.95	15.1	14.02	14.26	14.85	14.72
Sn Error	11.39	12.34	11.3	11.59	11.5	12.19
Bal	611712.06	676598.44	624594.38	623191.75	628849.25	633891.5
Bal Error	1226.19	1038.03	1173.26	1167.42	1132.77	1157.24
Nb	58.06	50.63	65.71	55.86	57.51	50.85
Nb Error	1.97	1.87	2.01	1.9	1.89	1.89
Bi	24.24	27.69	28.4	31.99	28.63	27.66
Bi Error	4.39	4.36	4.42	4.46	4.42	4.43
Al	29526.6	18847.55	27061.47	26933.02	26134.95	23539.08
Al Error	881.28	737.97	848.67	876.56	858.33	853.45
P	927.1	366.54	813.65	995.13	610.51	472.43
P Error	166.48	155.56	164.71	171.58	166.21	160.98
Si	299280.97	256543.48	291651.63	291881.78	291187.44	247057.19
Si Error	1384.75	1351.52	1378.49	1396.76	1387.33	1308.47

APPENDIX 2.

Character list modified from Shen et al. (2024) used in the presented cladistic analysis.

1. Premaxillae in adults: unfused (0); fused only rostrally (1); completely fused (2). (ORDERED)

2. Maxillary process of premaxilla: restricted to rostral portion (0); subequal or longer than facial contribution of maxilla (1).

3. Frontal process of premaxilla: short (0); relatively long, approaching rostral border of antorbital fenestra (1); very long, approaching the lacrimals (2). (ORDERED)

4. Premaxillary teeth: present throughout (0); present but rostral tip edentulous (1); present but restricted to rostral portion (2); absent (3).

5. Caudal margin of naris: far anterior than rostral border of antorbital fossa (0); nearly reaching or overlapping rostral border of antorbital fossa (1).

6. Naris longitudinal axis: considerably shorter than long axis of antorbital fossa (0); subequal or longer (1).

7. Maxillary teeth: present (0); absent (1).

8. Dorsal (ascending) ramus of maxilla: present with two fenestra (the promaxilllary and maxillary fenestra) (0); present with one fenestra (1); unfenestrated (2); ramus absent (3). (ORDERED)

9. Caudal margin of choana: located rostrally, not overlapping orbital region (0); displaced caudally, at same level or overlapping rostral margin of orbit (1).

10. Contact between palatine and maxilla/premaxilla: palatine contact maxilla only (0); contacts premaxilla and maxilla (1).

11. Jugal process of palatine: present (0); absent (1).

12. Ectopterygoid: present (0); absent (1).

13. Postorbital: present (0); absent (1).

14. Contact between postorbital and jugal: present (0); absent (1).

15. Quadratojugal: sutured to quadrate (0); joined through ligamentary articulation (1).

16. Lateral, round cotyla on mandibular process of quadrate (quadratojugal articulation): absent (0); present (1).

17. Squamosal incorporated into the braincase, forming a zygomatic process: absent (0); present (1).

18. Squamosal, zygomatic process: variably elongate, dorsally enclosing otic process of the quadrate and extending cranioventrally along shaft of this bone, dorsal head of quadrate not visible in lateral view (0); short, head of quadrate exposed in lateral view (1).

19. Frontal/parietal suture in adults: open (0); close, bones fully fused to one another (1).

20. Quadrate orbital process (pterygoid ramus): broad (0); sharp and pointed (1).

21. Quadrate pneumaticity: absent (0); present (1).

22. Quadrate: articulating only with squamosal (0); articulating with both prootic and squamosal (1).

23. Otic articulation of the quadrate: articulates with a single facet (squamosal) (0); articulates with two distinct facets (prootic and squamostal) (1); articulates with two distinct facets and quadrate differentiated into two heads (2). (ORDERED)

24. Quadrate distal end: with two transversely aligned condyles (0); with a triangular, condylar pattern, usually composed of three distinct condyles (1).

25. Eustachian tubes: paired, lateral, and well-separated from each other (0); paired, close to each other and to cranial midline or forming a single cranial opening (1).

26. Dentary teeth: present (0); absent (1).

27. Robustness of teeth relative to dentary: anteroposterior width of largest tooth crowns (measured at thickest portion of crown's base) far less than half of dentary dorsoventral depth (0); close to half (or more) of dentary depth, i.e., 45%, or more (1). Taxa near the cutoff point are coded 0/1.

28. Dentary tooth implantation: teeth in individual sockets (0); teeth in a communal groove (1).

29. Symphysial portion of dentaries: unfused (0); fused (1).

30. Deeply notched rostral end of mandibular symphysis: absent (0); present (1).

31. Small ossification present at rostral tip of mandibular symphysis (intersymphysial ossification or "predentary bone"): absent (0); present (1).

32. Caudal margin of dentary: unforked, or with weakly developed dorsal ramus (0); strongly forked with dorsal and ventral rami approximately equal in caudal extent (1).

33. Meckel's groove of mandible (medial side of mandible): not completely covered by splenial (0); covered by splenial, not exposed medially (1).

34. Rostral mandibular fenestra: absent (0); present (1).

35. Caudal mandibular fenestra: present (0); absent (1).

36. Articular pneumaticity: absent (0); present (1).

37. Atlantal hemiarches in adults: unfused (0); fused, forming a single arch (1).

38. One or more pneumatic foramina piercing centra of mid-cranial cervicals, caudal to level of parapophysis-diapophysis: present (0); absent (1).

39. Cervical vertebrae: variably dorsoventrally compressed, amphicoelous ("biconcave": flat to concave articular surfaces) (0); cranial articular surface heterocoelous (i.e., mediolaterally concave, dorsoventrally convex), caudal articular surface flat or slightly concave (1); heterocoelous cranial (i.e., mediolaterally concave, dorsoventrally convex) and caudal (i.e., mediolaterally convex, dorsoventrally concave) articular surfaces (2). (ORDERED)

40. Prominent carotid processes in intermediate cervicals: absent (0); present (1).

41. Postaxial cervical epipophyses: prominent, projecting further back from postzygapophyses (0); weak, not projecting further back from postzygapophyses, or absent (1).

42. Keel-like ventral surface of cervical centra: absent (0); present (1).

43. Prominent (50% or more the height of centrum's cranial articular surface) ventral processes of cervicothoracic vertebrae: absent (0); present (1).

44. Thoracic vertebral count: 13–14 (0); 11–12 (1); fewer than 11 (2). The transition between cervical and thoracic vertebrae is often difficult to identify, which makes counting these vertebrae problematic; we identify the first vertebra in articulation with a long costal rib as the first thoracic vertebra (ORDERED)

45. Thoracic vertebrae: at least part of series with subround, central articular surfaces (e.g., amphicoelous/opisthocoelous) that lack the dorsoventral compression seen in heterocoelous vertebrae (0); series completely heterocoelous (1).

46. Thoracic vertebrae, lateral side of centra: weakly or not excavated (0); deeply excavated by a groove (1); excavated by a broad fossa (2).

47. Cranial thoracic vertebrae, parapophyses: located in cranial part (0) or central part (1) of centra.

48. Sacral vertebrae, number ankylosed centra (synsacrum): less than 7 (0); 7 (1); 8 (2); 9 (3); 10 (4); more than 10 (5). (ORDERED)

49. Synsacrum, procoelous articulation with last thoracic centrum (deeply concave facet of synsacrum receives convex articulation of last thoracic centrum): absent (0); present (1).

50. Cranial vertebral articulation of first sacral vertebra: approximately equal in height and width (0); wider than high (1).

51. Degree of fusion of distal caudal vertebrae: fusion absent (0); few vertebrae partially ankylosed (intervening elements are well-discernable) (1); vertebrae completely fused into a pygostyle (2). (ORDERED)

52. Distal caudal vertebra prezygapophyses: elongate, exceeding the length of centrum by more than 25% (0); shorter (1); absent (2). (ORDERED)

53. Pygostyle: longer than or equal to the combined length of free caudals (0); shorter (1).

54. Cranial end of pygostyle dorsally forked: absent (0); present (1).

55. Cranial end of pygostyle with a pair of laminar, ventrally projected processes: absent (0); present (1).

56. Distal constriction of pygostyle: absent (0); present (1).

57. Ossified uncinate processes in adults: absent (0); present and free (1); present and fused (2).

58. Gastralia: present (0); absent (1).

59. Coracoid shape: rectangular to trapezoidal in profile (0); strutlike (1).

60. Coracoid-scapula articulation: "ball and socket" articulation (i.e., pit-shaped scapular cotyla developed on coracoid, and coracoidal tubercle developed on scapula) (0); scapular articular surface of coracoid convex (1); flat (2).

61. Scapula: articulated at omal end of coracoid (0); well below it (1).

62. Coracoid, humeral articular facet (glenoid): dorsal to acrocoracoid process ("biceps tubercle") (0); ventral to acrocoracoid process (1).

63. Humeral articular facets of coracoid and scapula: placed in same plane (0); forming a sharp angle (1).

64. Coracoid, acrocoracoid: straight (0); hooked medially (1).

65. Coracoid, laterally compressed omal end with nearly aligned acrocoracoid process, humeral articular surface, and scapular facet, in dorsal view: absent (0); present (1).

66. Coracoid, procoracoid process: absent (0); present (1).

67. Coracoid, broad, deep fossa on dorsal surface (dorsal coracoidal fossa): absent (0); present (1).

68. Coracoid, supracoracoidal nerve foramen: centrally located (0); displaced toward (often as an incisure) medial margin (1); absent (i.e., nerve position is displaced so that it no longer passes through coracoid) (2). (ORDERED).

69. Coracoid, medial surface, strongly depressed elongate furrow (usually levelled with passage of n. supracoracoideus): absent (0); present (1).

70. Coracoid, width of the sternal end relative to the length along the shaft: approximately half or greater (0); between half to 1/3 (1); less than 1/3 (2).

71. Coracoid, sternal margin: convex (0); nearly straight (1); concave (2)

72. Coracoid, supracoracoid nerve foramen, location relative to dorsal coracoidal fossa: above fossa (0); inside fossa (1).

73. Coracoid, sternolateral corner: unexpanded (0); expanded (1); well developed squared-off lateral process (sternocoracoidal process) (2); present and with distinct omal projection (hooked) (3).

74. (244) Scapula and coracoid: fused (0); unfused (1).

75. Scapula, blade: straight (0); sagittally curved (1).

76. Scapula, length: shorter than humerus (0); as long as or longer than humerus (1).

77. (245) Scapula, acromion process length relative to length of humeral articular facet: less than half (0); nearly equivalent (1); longer but less than two times (2); more than two times longer (3). (ORDERED)

78. Scapula, acromion process: in lateral or costal view, strongly projecting craniodorsally, forming a large angle with proximal shaft (0); nearly parallel to shaft (1).

79. Scapula, costal surface of blade with prominent longitudinal furrow: absent (0); present (1).

80. Scapula, caudal end: blunt (may or may not be expanded) (0); sharply tapered (1).

81. Furcula: boomerang-shaped (0); V to Y-shaped (1); U-shaped (2).

82. Furcula, interclavicular angle: approximately 90° (0); less than 70° (1). The interclavicular angle is measured as the angle formed between three points: the omal ends of the rami and the center of the clavicular symphysis.

83. Furcula, dorsal and ventral margins: subequal in width (0); ventral margin distinctly wider than dorsal margin so that furcular ramus appears concave laterally (1).

84. Furcula, hypocleideum: absent (0); present as a tubercle or short process (1); present as elongate process approximately 30–50% the length of rami (2); hypertrophied, exceeding 50% the length of rami (3). (ORDERED)

85. Sternum: unossified (0); partially ossified, coracoidal facets cartilaginous (1); fully ossified (2).

86. Sternum, ossification: two flat bony plates (0); single, more or less flat element (1); single element, with slightly raised midline ridge (2); single element, with strongly projected carina (3). (scorings revised)

87. Sternum, carina: near to, or projecting rostrally from, cranial border (0); not reaching cranial border (1).

88. Sternum, caudal margin, number of paired caudal trabeculae: none (0); one (1); two (2).

89. Sternum, outermost trabeculae: tips terminate cranial to caudal end of sternum (0); tips terminate at or approaching caudal end of sternum (1); tips extend caudally past the end of sternal midline (2).

90. Sternum, distal expansion of outermost trabecula: absent (0); present, simple bulb-like (1); fan-shaped (2); triangular–shaped with acute medial angle (3); branched (4).

91. Sternum, rostral margin broad and rounded: absent (0); present (1).

92. Sternum, coracoidal sulci spacing on cranial edge: widely separated mediolaterally (0); adjacent (1); crossed on midline (2). In taxa such as Eoalulavis in which the preserved sternum does not bear actual sulci, the placement of the coracoids (seemingly in their original place) can be used to infer their position relative to the sternum.

93. Sternum, costal facets: absent (0); present (1).

94. Sternum, caudal half, paired enclosed fenestra: absent (0); present (1).

95. Sternum, dorsal surface, pneumatic foramen (or foramina): absent (0); present (1).

96. (243) Sternum, outermost trabecula: mainly parallel to long axis of sternum (0); clearly directed caudolaterally (1).

97. Humerus, proximal and distal ends: twisted (0); nearly co-planar (1)

98. Humerus, head: concave cranially and convex caudally (0); globe shaped, craniocaudally convex (1).

99. Humerus, proximal margin of head is convex in its central portion, rising ventrally and dorsally: absent (0); present (1). (MODIFIED)

100. Humerus, proximocranial surface, well-developed circular fossa on midline: absent (0); present (1).

101. Humerus, transverse ligamental groove: absent (0); present (1).

102. Humerus, ventral tubercle projected caudally, separated from humeral head by deep capital incision: absent (0); present (1).

103. Humerus, pneumatic fossa in caudoventral corner of proximal end: absent or rudimentary (0); well developed (1).

104. Humerus, deltopectoral crest: projected dorsally (the plane of the crest is coplanar to cranial surface of humerus) (0); projected cranially (1).

105. Humerus, deltopectoral crest width: less than shaft width (0); approximately same width (1); prominent and subquadrangular (i.e., subequal length and width) (2).

106. Humerus, deltopectoral crest, distal end recedes abruptly with the humeral shaft: present (0); absent (1)

107. Humerus, deltopectoral crest: imperforated (0); perforated by a fenestra (1).

108. Humerus, bicipital crest: little to no cranial projection (0); developed as cranial projection relative to shaft surface in ventral view (1); hypertrophied, rounded tumescence (2).

109. Humerus, distal end of bicipital crest, pit-shaped fossa for muscular attachment: absent (0); craniodistal on bicipital crest (1); directly ventrodistal at tip of bicipital crest (2); caudodistal, variably developed as a fossa (3).

110. Humerus, demarcation of muscle origins (e.g., m. extensor metacarpi radialis) on the dorsal edge of the distal humerus: no indication (0); a pit or a tubercle (1); a variably projected scar-bearing tubercle (dorsal supracondylar process) (2).

111. Humerus, well-developed brachial depression on cranial face of distal end: absent (0); present (1).

112. Humerus, well-developed olecranon fossa on caudal face of distal end: absent (0); present (1).

113. Humerus, groove for passage of m. scapulotriceps: absent (0); present (1).

114. Humerus, m. humerotricipitalis groove: absent (0); present as a well-developed ventral depression contiguous with the olecranon fossa (1).

115. Humerus, distal margin: approximately perpendicular to long axis of shaft (0); strongly angled ventrally (ventrodistal margin projected significantly distal to dorsodistal margin) (i.e., well-projected flexor process (1).

116. Humeral distal condyles: mainly located on distal aspect (0); on cranial aspect (1).

117. Humerus, long axis of dorsal condyle: at low angle to humeral axis, proximodistally oriented (0); at high angle to humeral axis, almost transversely oriented (1).

118. Humerus, distal condyles: subround, bulbous (0); weakly defined, “straplike” (1).

119. Humerus, ventral condyle: length of long axis less than the same measure in dorsal condyle (0); same or greater (1).

120. Ulna: shorter than humerus (0); nearly equivalent to or longer than humerus (1).

121. Ulna: mid-shaft relative width: radial-shaft/ulnar-shaft ratio larger than 0.70 (0); smaller than 0.70 (1).

122. Ulna, cotylae: dorsoventrally adjacent (0); widely separated by deep groove (1).

123. Ulna, dorsal cotyla strongly convex: absent (0); present (1).

124. Ulna, bicipital scar: absent (0); developed as slightly raised scar (1); developed as conspicuous tubercle (2).

125. Ulna, proximal end with well-defined area for insertion of m. brachialis anticus: absent (0); present (1).

126. Ulna, semilunate ridge on dorsal condyle: absent (0); present (1).

127. Radius, long longitudinal groove on ventrocaudal surface of shaft: absent (0); present (1).

128. Ulnare: heart-shaped with little differentiation into short rami (0); U-shaped to V-shaped, well-developed rami (1).

129. Semilunate carpal and proximal ends of metacarpals in adults: unfused (0); semilunate fused to the alular (I) metacarpal (1); semilunate fused to the major (II) and minor (III) metacarpals (2); fusion of semilunate and all metacarpals (3). Juvenile specimens are scored as “?” to account for the possibility of ontogenetic change.

130. Semilunate carpal, position relative to alular metacarpal (I): over entire proximal surface (0); over less than one-half proximal surface or no contact present (1).

131. Carpometacarpus, proximal ventral surface: flat (0); raised ventral projection contiguous with minor metacarpal (1); pisiform process forming a distinct peg-like projection (2).

132. Carpometacarpus, proximoventral surface, supratrochlear fossa deeply excavating proximal surface of pisiform process: absent (0); present (1).

133. Alular metacarpal (I), round-shaped: absent (0); present (1).

134. Alular metacarpal (I), extensor process: absent (0); tip barely (1) or conspicuously (2) surpasses cranial margin of distal articular facet. (ORDERED)

135. Alular metacarpal (I), distal articulation with proximal phalanx: ginglymoid (0); shelf (1); ball-like (2).

136. Minor metacarpal (III), craniocaudal diameter as percentage of same dimension of major metacarpal (II): approximately equal or greater than 50% (0); less than 50% (1).

137. Alular digit (I), proximal phalanx: longer than proximal phalanx of major digit (II) (0); shorter than or equivalent to proximal phalanx of major digit (II) (1).

138. Intermetacarpal process (or tubercle) on major metacarpal (II): absent (0); present (1).

139. Intermetacarpal space: absent or very narrow (0); at least as wide as maximum width of minor metacarpal (III) shaft (1).

140. Intermetacarpal space: reaches proximally as far as distal end of alular metacarpal (I) (0); terminates distal to end of alular metacarpal (I) (1). (scorings revised)

141. Distal end of metacarpals: unfused (0); partially or completely fused (1).

142. Minor metacarpal (III) projecting distally more than major metacarpal (II): absent (0); present (1).

143. Alular digit (I), proximal phalanx, distal extension relative to major metacarpal (II): beyond distal end of major metacarpal (II) (0); approximately equal in distal extension (1); shorter than distal end but beyond half of major metacarpal (II) (2); terminating less than half of major metacarpal (II) (3). (ORDERED)

144. Proximal phalanx of major digit (II): round-shaped cross section (0); flat and craniocaudally expanded (1).

145. Intermediate phalanx of major digit (II): longer than proximal phalanx (0); shorter than or equivalent to proximal phalanx (1).

146. Ungual phalanx of major digit (II): present (0); absent (1).

147. Ungual phalanx of major digit (II): larger or subequal to other manual unguals (0); smaller than alular ungual but larger than ungula phalanx of minor (III) digit (ungual of minor digit may or may not be present) (1); smaller than unguals of alular and minor digits (2).

148. Ungual phalanx of minor digit (III): present (0); absent (1).

149. Manus, relative length: length of semilunate carpal + major metacarpal and digit longer than humerus (0); subequal (1); shorter (2). (ORDERED)

150. Intermembral index = (length of humerus + ulna)/(length of femur + tibiotarsus): less than 0.7 (0); between 0.7 and 0.9 (1); between 0.9 and 1.1 (2); greater than 1.1 (3).

151. Pelvis, bone fusion at level of acetabulum: unfused or partial fusion (0); completely fused (1). Juvenile specimens with unfused pelvis are scored "?" to allow for ontogenetic fusion.

152. Ilium/ischium, distal co-ossification to completely enclose ilioischiadic fenestra: absent (0); present (1).

153. Ilium, midline proximity of preacetabular wings: separated (may exist cartilaginous connection) (0); co-ossified, dorsal closure of “iliosynsacral canals” (1).

154. Preacetabular pectineal process (preacetabular tubercle of Baumel): absent (0); present (1).

155. Pelvis, acetabulum proportions: large acetabulum, acetabulum/ilium length ratio greater than 0.11 (0); small acetabulum, same proportion equal or smaller than 0.11 (1).

156. Prominent antitrochanter: caudally directed (0); caudodorsally directed (1).

157. Ilium, postacetabular process: deep (0), more than 50% of depth of preacetabular wing at level of acetabulum; shallow (1), less than 50%.

158. Ilium, brevis fossa: present (0); absent (1).

159. Ischium, relative length: two-thirds or less the length of pubis (0); more than two-thirds the length of pubis (1).

160. Ischium, obturator process: prominent (0); reduced or absent (1). 1

161. Ischium, proximodorsal (or proximocaudal) process: absent (0); present (1).

162. Pubis, orientation of proximal portion: cranially to subvertically oriented (0); retroverted, separated from main synsacral axis by a 45–65° angle (1); more or less parallel to ilium and ischium (2). (ORDERED)

163. Ilium, pubic pedicel very compressed laterally and hook-like: absent (0), present (1).

164. Pubis, shaft laterally compressed throughout its length: absent (0); present (1).

165. Pubis, pubic apron: present (0); absent (absence of symphysis) (1).

166. Pubis, distal foot: flaring into simple round shape (0); triangular shape with pointed caudal tip and caudoventally directed with respect to distal pubic shaft (1); caudal tip recurved caudodorsally with respect to distal pubic shaft (2); absent (3).

167. Femur, distinct fossa for capital ligament: absent (0); present (1).

168. Femur, neck: present (0); absent (1).

169. Femur, anterior trochanter: separated from greater trochanter (0); fused to it, forming a trochanteric crest with laterally curved edge (1); fused to it, forming a trochanteric crest with flattened edge (2).

170. Femur, trochanteric crest: projects proximally beyond femoral head (0); equal in proximal projection (1); does not project beyond femoral head (2).

171. Femur, posterior trochanter: present, developed as slightly projected tubercle or flange (0); hypertrophied, “shelf-like” conformation (1); absent (2).

172. Femur, prominent patellar groove: absent (0); present as continuous extension onto distal shaft (1); present and separated from shaft by slight ridge, giving it a pocketed appearance (2).

173. Femur, lateral distal end: ectocondylar tubercle and lateral condyle separated by deep notch (0); ectocondylar tubercle and lateral condyle contiguous but without developing a tibiofibular crest (1); tibiofibular crest present, defining laterally a fibular trochlea (2). (ORDERED)

174. Femur, popliteal fossa distally bounded by a complete transverse ridge: absent (0); present (1).

175. Tibia, calcaneum, and astragalus: unfused or poorly co-ossified (sutures still visible) (0); complete fusion of tibia, calcaneum, and astragalus (1).

176. Tibia, round proximal articular surface: absent (0); present (1).

177. Tibia, proximal articular surface: flat (0); angled so that medial margin is elevated with respect to lateral margin (1).

178. Tibiotarsus, proportions: tibiotarsus length/tarsometatarsus length equals 2 or more (0); between 2 and 1.6 (1); smaller than 1.6 (2). When distal tarsals are not fused with metatarsals, metatarsal III length is used.

179. Tibiotarsus, cnemial crests: absent (0); present, one (1); present, two (2).

180. Tibia, caudal extension of articular surface for tarsals/tarsometatarsus: absent, articular surface restricted to distalmost edge of caudal surface (0); well-developed caudal extension, sulcus cartilaginis tibialis (Baumel & Witmer, 1993), distinct surface extending up caudal surface of tibiotarsus (1); with well-developed, caudally projecting medial and lateral crests (2). (ORDERED)

181. Tibiotarsus, extensor canal: absent (0); present as emarginate groove (1); groove bridged by ossified supratendinal bridge (2). (ORDERED)

182. Tibibiotarsus, condyles, cranial projection: medial condyle projecting farther cranially than lateral condyle (0); equal in cranial projection (1).

183. Tibiotarsus, condyles, relative mediolateral width: medial condyle wider (0); approximately equal (1); lateral condyle wider (2). (ORDERED).

184. Tibiotarsus, condyles, intercondylar groove: mediolaterally broad, approximately 1/3 with of anterior surface (0); less than 1/3 width of anterior surface (1).

185. Tibiotarsus, condyles: gradual sloping of condyles towards tibiotarsal midline of tibiotarsus (0); no tapering of either condyle (1).

186. Fibula, proximal end: prominently excavated by medial fossa (0); nearly flat (1).

187. Fibula, tubercle for m. iliofibularis: craniolaterally directed (0); laterally directed (1); caudolaterally or caudally directed (2). (ORDERED)

188. Fibula, distal end reaching proximal tarsals: present (0); absent (1).

189. Distal tarsals in adults: free (0); completely fused to the metatarsals (1). Juvenile specimens are scored as "?" in order to account for the possibility of ontogenetic change.

190. Metatarsals II–IV, intermetatarsal fusion: absent or minimal co-ossification (0); partial fusion, sutural contacts easily discernible (1); completely or nearly completely fused, sutural contacts absent or poorly demarcated (2). (ORDERED)

191. Metatarsal V: present (0); absent (1).

192. Metatarsal III, proximal end: co-planar with metatarsals II and IV (0); plantarly displaced with respect to metatarsals II and IV (1).

193. Tarsometatarsus, proximal vascular foramen and/or foramina between metatarsals III and IV: absent (0); one (1); two (2).

194. Tarsometatarsus, intercotylar eminence: absent (0); present, low and rounded (1); present, high and peaked (2).

195. Tarsometatarsus, projected surface and/or grooves on proximocaudal surface (associated with the passage of tendons of pes flexors; hypotarsus): absent (0); developed as caudal projection with flat caudal surface (1); at least one groove enclosed by bone caudally (2). (ORDERED)

196. Tarsometatarsus, plantar surface: flat (0); excavated (1).

197. Tarsometatarsus, distal vascular foramen completely enclosed by metatarsals III and IV: absent (0); present (1).

198. Metatarsal I: straight (0); J-shaped, with short projection (articulation of hallux) extending medially (1); J-shaped; articulation of hallux extending caudally (2); distal half of metatarsal I is laterally deflected so that laterodistal surface is concave (3).

199. Metatarsal II tubercle (associated with the insertion of the tendon of the m. tibialis cranialis): absent (0); present, approximately centered on proximodorsal surface of metatarsal II (1); present, developed on lateral surface of metatarsal II, at contact with metatarsal III or on lateral edge of metatarsal III (2).

200. Metatarsal II, distal plantar surface, fossa for metatarsal I: absent (0); shallow notch (1); conspicuous ovoid fossa (2). (ORDERED)

201. Relative position of metatarsal trochleae: trochlea III more distal than trochleae II and IV (0); trochlea III at same level as trochlea IV, both more distal than trochlea II (1); trochlea III at same level as trochleae II and IV (2); distal extent of trochlea III intermediate to trochlea IV and II where trochlea IV projects furthest distally (3).

202. Metatarsal II, distal extent of metatarsal II relative to metatarsal IV: approximately equal in distal extent (0); metatarsal II shorter than metatarsal IV but reaching distally farther than base of metatarsal IV trochlea (1); metatarsal II shorter than metatarsal IV, reaching distally only as far as base of metatarsal IV trochlea (2).

203. Tarsometatarsus, trochlea in distal view: aligned in a single plane (0); metatarsal II slightly displaced plantarly with respect to III and IV (1); metatarsal II strongly displaced plantarly in respect to III and IV, such that there is little or no overlap in medial view (2).

204. Metatarsal II, trochlea of metatarsal II broader than trochlea of metatarsal III: absent (0); present (1).

205. Metatarsal III, trochlea in plantar view, proximal extent of lateral and medial edges of trochlea: trochlear edges approximately equal in proximal extent (0); medial edge extends farther (1).

206. Distal end of metatarsal II strongly curved medially: absent (0); present (1).

207. Phalanx in digit IV; second and third phalanges reduced and significantly shorter than fourth phalanx: absent (0), present (1), present, but with proximal phalanx reduced to be nearly equal in length with second and third phalanx (2).

208. Digit IV phalanges in distal view, medial trochlear rim enlarged with respect to lateral trochlear rim: absent (0); present, lateral trochlea reduced to a rounded peg (1).

209. Pes, proximal phalanx of hallux is the longest non-ungual phalanx: absent (0); present (1).

210. Size of claw of hallux relative to other pedal claws: shorter, weaker, and smaller (0); similar in size (1); longer, more robust, and larger (2).

211. Alula: absent (0); present (1).

212. Fan-shaped feathered tail composed of more than two elongate retrices: absent (0); present (1).

APPENDIX 3.

Character matrix for the cladistic analysis of STM7-156. To access the NEX file, go to:
https://palaeo-electronica.org/content/2025/5712-longipterygid-enantiornithine-chromeornis